Design of a Beam-Steerable Microstrip Line based Leaky Wave Antenna using Uniaxial Field Programmable Microwave Substrate (FPMS)

by

Noben Kumar Roy

A thesis presented to the
Lakehead University in partial
fulfilment of the required degree of

Master of Science

in

Electrical and Computer Engineering

Faculty of Engineering
Lakehead University
Thunder Bay, Ontario, Canada

May 2021

ABSTRACT

The ever-growing wireless technologies of today are pushing the limits of the state-of-the-art radio frequency (RF) components design. One special requirement which is widely needed in modern applications is for the RF components to be smart, compact, and agile. Performance characteristics such as frequency tunability, antenna pattern reconfigurability, radiation polarization diversity etc., are the need of the hour. Field Programmable Microwave Substrate (FPMS) is a pertinent answer to the challenges of the modern wireless communication standards. Given the unprecedented level of programmability, the FPMS has the potential to affect the RF and microwave component design in a similar manner as the Field Programmable Gate Array (FPGA) affected the digital domain. The FPMS technology is composed of small unit cells that can be actively biased to control the dielectric material characteristics. Using this quality of FPMS, this work focuses on the design of a leaky wave antenna (LWA) where the uniaxial modulation of the substrate properties allows for the beam steering capabilities.

The antenna is designed to operate at 2 GHz on a Duroid 5880 material system as a proof-of-concept. First, the FPMS unit cell is optimized to operate at the desired frequency of 2 GHz with the help of a full wave solver ANSYS HFSS. Once optimized, the unit cells are integrated onto the antenna structure to study the effects on its radiation and impedance performance. A complete parametric study is performed on various design parameters to obtain the optimized impedance and radiation performance of the antenna. The low loss nature of the substrate provides for an antenna gain value as high as 11 dBi with a gain variation of 2.5 dB. A continuous maximum beam steering of backward and forward direction i.e., ±30° is achieved from the LWA design with

reasonable gain values. These performance parameters of the antenna demonstrate the potential of the novel FPMS technology in the design of intelligent RF components.

Keywords: Microstrip Antenna; Leaky Wave Antenna (LWA); Field Programmable Microwave Substrate (FPMS).

ACKNOWLEDGEMENT

I would like to express my heartfelt gratitude to Farhan Abdul Ghaffar, my thesis supervisor, for his valuable support, encouragement, and guidance throughout my thesis journey. Thank you so much for your belief and trust in me. I have learned how to be a smart researcher and a more well-rounded person, thanks to your guidance. You were always there for me whenever I needed you, with such a positive attitude that allowed me to bring out my hidden inquisitiveness and push it to the very limit, for which I will be eternally grateful. You gave my life a new direction, and the success of this work would not have been possible without you.

I am also grateful to my incredible parents, Poritosh Roy and Lishi Natu, my aunt Ngawang Pema, and my lifelong friend Tenzing Lhadon for your generous support. What I am today is entirely due to you people, and none of this would have been possible without you all.

Finally, I would like to thank Sahin and Mohamed for their assistance, as well as the CMC Microsystems team members for their help and support with the Ansys software for simulations.

TABLE OF CONTENT

LIST OF FIGURES

Chapter 1

Chapter 2

Chapter 3

Chapter 4

Chapter 5

Chapter 1

Introduction

1.1 Motivation

Reconfigurable antennas have been used for decades in applications such as military radars, deep space communication, cellular technology, and others where the connected devices move relative to one another [1]. For instance, in military radars, the antenna on the flying aircraft must always be connected to the stationary base station through a wireless link as shown in Fig. 1.1. This can be accomplished with the help of reconfigurable antennas. Reconfigurability in antennas can be attributed to their impedance as well as radiation performance [2], [3].

(a) (b) (c)

Fig. 1. 1: Application of reconfigurable antenna (a) Military radar (b) Fighter aircraft (c) Military base station [2]

In terms of radiation performance, a widely used property is the beam steering of antennas, also referred to as phased array antennas. Just like the classical applications, beam reconfigurable

antennas find their application in many of the modern wireless systems. However, these modern applications have their own set of demands. These include compact size, agility, reconfigurability, low-cost and last but not the least, high efficiency. A couple of examples of these applications: on-the-go satellite communication and connected vehicles are shown in Fig. 1.2 [5].

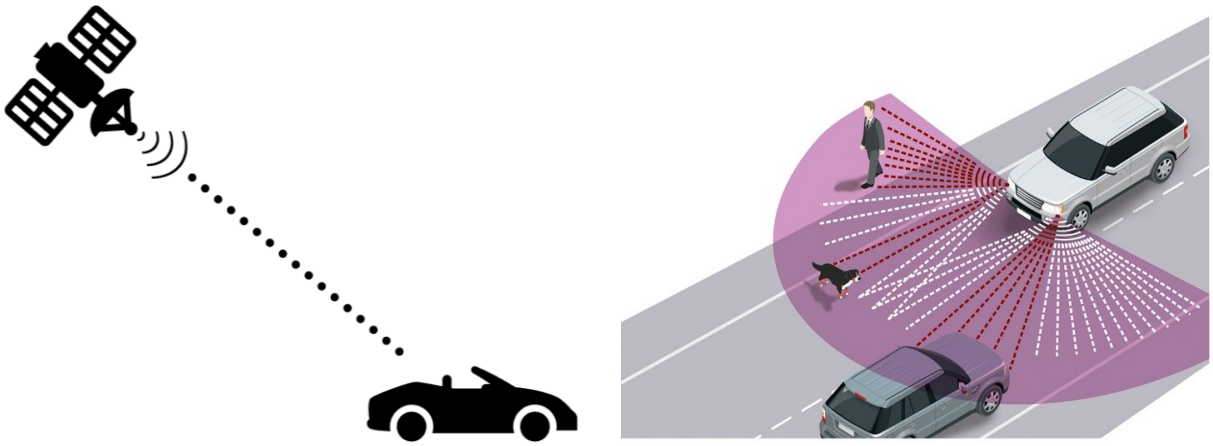

(a) (b)

Fig. 1. 2: Modern Application (a) On-the-go Satellite Communication (b) Automotive Radars [5]

On-the-go satellite communication is demonstrated in Fig. 1.2(a), where the satellite and the connected vehicle (car) are moving relative to one another. Because of the relative motion between the satellite and the car, the system requires reconfigurable antennas that can establish a continuous connection between the two. Similarly, the emergence of self-driven cars as a concept, has increased the importance of reconfigurable antenna's systems manifolds. In such an application, the car is equipped with automotive radars/sensors all around it in order to detect any obstruction, such as a person, animal, or other vehicles approaching it to provide collision mitigation.

Eventually, the goal is to make sure that the car can not only detect obstacles around it, but it can at the same time communicate with the infrastructure so as to materialize the dream of self-driven cars where the communication link acts as the driver of the vehicle.

All the applications outlined above (including new and old) require smart antennas for their practical realization. For wireless communication, there is a variety of antennas available, each of which is more or less effective for a specific application. Since single antenna characteristics are fixed, system performance is restricted in the event of a change in scenario or in a system that runs multiple applications at the same time. This can be strengthened by using several antennas while sacrificing device size, or by having the antenna reconfigurable so that its features can be adjusted as the system requirements change. Hence, a single reconfigurable antenna can replace multiple conventional/classical antennas. The most popular types of reconfigurable antennas are frequency reconfigurable and radiation pattern reconfigurable antennas.

Frequency tunable antennas are designed to vary their center frequency as per the requirements [3], [7]. These are useful in situations where several communications systems overlap in one solution. A good example of such an application is cell-phone communication, where standards such as Wi-Fi, GPS, Cellular Communication are all integrated into a single unit.

Similarly, radiation pattern reconfigurability can be achieved by an intentional modification of the antenna radiation's spherical distribution. The most advanced and well-known application in this case is beam steering, which includes steering the trajectory of the maximum radiation (main lobe) to optimised antenna gain in a particular direction. The direction of this maximum gain can be altered as per the user requirement. Among others, one of the most commonly used beam steerable antennas is known as Leaky Wave Antennas (LWAs) [6]. LWAs belong to a special class of antennas known as traveling wave antenna where the beam of the antenna is steered by varying

the frequency of the applied radio frequency (RF) signal [7]. Some of the practical applications where change in frequency is an advantageous are Photonic Radar System [8] and Multimode Adaptable Microwave Radar Sensor [9]. LWAs enable beam steering in photonic radar systems by estimating the direction of arrival of radar echoes for detection and localization of multiple objects by using a frequency modulated continuous wave signal. In the case of a multimode microwave radar system, the LWAs were used in military vehicles to identify and track target (threatening missiles) while generating signals to determine the appropriate counter-measure reaction.

However, many of the wireless applications, such as on-the-move satellite systems, self-driven cars etc., would not want to change the center frequency of the antenna while the antenna's beam is steered. Therefore, the focus of this thesis is on the design of a fixed frequency beam steerable LWA using a novel technology known as 'Field Programmable Microwave Substrate (FPMS)' [36]. It is for the first time, that the FPMS is explored as a viable option for the design and implementation of smart antenna systems. FPMS is composed of individual unit cells that can locally control the dielectric properties of a medium. This makes it an excellent candidate for design of LWAs which rely on the progressive properties of the substrate to achieve the desired radiation characteristics. The simulated results of the LWA design readily validates the use of the FPMS technology in the design of reconfigurable antenna elements.

1.2 Thesis Objectives

The goals of this thesis can be summarized as follows:

- To study and optimize the FPMS unit cell design on a low dielectric constant substrate such as Duroid 5880 ($\varepsilon_r = 2.2$) to ensure the realization of an efficient antenna element.

- Uniaxial integration of the FPMS unit cells in a microstrip line based leaky wave antenna (MLWA) to demonstrate its beam steering in one plane.
- To show continuous beam steering on either side of the boresight radiation, i.e., forward and backward direction while maintaining radiation performance.
- As a proof-of-concept, the thesis is to focus on 2 GHz (within S-Band) for the antenna realization (targeting satellite communication), however, the concept can be easily translated to higher frequencies to cater for other wireless applications.

1.3 Thesis Contribution

Following contributions can be outlined from the proposed thesis research:

- This work presents the design of the first-ever leaky wave antenna based on FPMS technology for radiation pattern reconfigurability.
- A beam steering range of ±30° is achieved from the full-wave simulations carried out in an electromagnetic (EM) simulator (Ansys High Frequency Structure Simulator, HFSS).
- The antenna provides a maximum gain of 11 dBi with a gain variation of 2.5 dB when the main-beam is steered to a maximum of ±30° i.e., on either side of boresight.
- The antenna maintains its impedance performance to match accordingly to the reference of IEEE journal papers, i.e., reflection coefficient $|\Gamma| \leq -10$ dB while reconfiguring its radiation pattern.

1.4 Thesis Organization

The thesis organization can be outlined as:

Chapter 2 provides an overview of the theory behind the leaky wave antennas (LWA). It covers the basic working principles, and the physics behind its operation. This is followed by an extensive

literature review on various LWAs to summarize the state-of-the-art that currently exists in this domain.

Chapter 3 begins with an introduction to the FPMS technology and its unit cells that are needed to realize it. This is followed by a detailed discussion on the optimization of the FPMS unit cells with respect to the dielectric constant and the resonant frequency, which is done by varying different design parameters and studying the impedance results.

The main contribution of this thesis, i.e., FPMS based LWA, is explained in Chapter 4. At first, the chosen antenna design is optimized to work at 2 GHz with the help of a full wave solver ANSYS HFSS. The integration of the optimized FPMS unit cells along one of the axis of the antenna is then carried out. Followed by a complete parametric study is performed on various design parameters to obtain the best possible impedance and radiation performance of the antenna.

Finally, the thesis concludes by listing the contributions of this work and highlighting some of the future steps that are currently undertaken to validate the proposed design in measurements. Furthermore, other research directions on the antenna designs using FPMS technology are also explained briefly to hint at possible future initiatives.

Chapter 2

Background and Literature Review

As discussed in Chapter 1, the focus of the thesis is on the design of beam-steerable/reconfigurable antennas. For this purpose, leaky wave antenna has been chosen as the preferred candidate. Thus, it is pertinent to discuss some fundamentals of the leaky wave antenna and to present some designs that already exist in literature before dwelling into the actual antenna design.

2.1 Introduction

Leaky-wave antennas (LWA) can be broadly classified in the category of traveling wave antennas. LWA uses a guiding structure that supports wave propagation along the length, with the wave radiating or "leaking" continuously along the structure. This kind of performance is achieved by carefully modulating the wave impedance along the antenna length. LWAs may be uniform, quasi-uniform, or periodic depending upon the design topology. The slitted rectangular waveguide, developed by W. W. Hansen in 1940, is the first known LWA ever presented [6]. This antenna design provided a new platform to carry out research in the domain of traveling wave antennas. Most of the early designs of this category of antenna rely on closed waveguides, with leakage achieved by inserting long uniform slits or a series of closely spaced holes into the waveguides to allow power to radiate [10]-[16]. As suggested by Hines and Upson [6], by introducing a series of closely spaced holes into the waveguide structure, the antenna can be designed to radiate power along its length, as illustrated in Fig. 2.1. The beamwidth and directivity of the antenna can be controlled by the size, number and spacing between the slits.

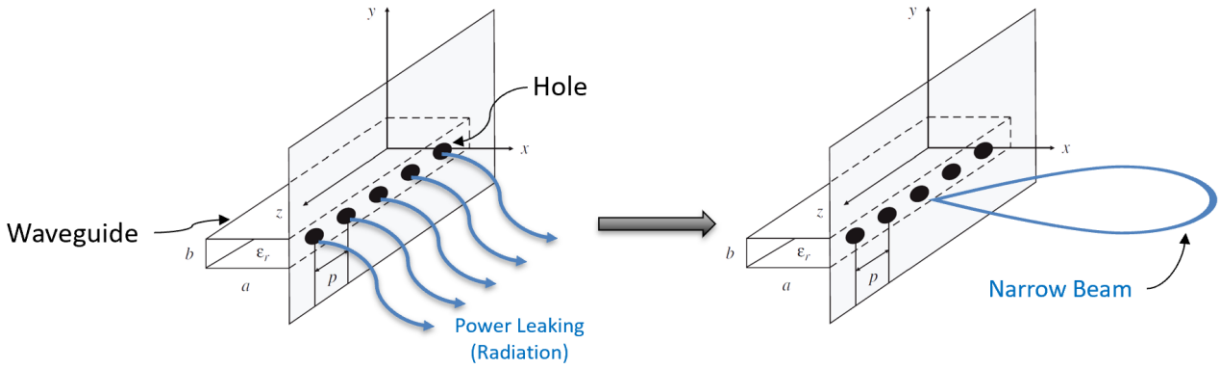

Fig. 2. 1: A periodic leaky-wave antenna with a rectangular waveguide and a periodic array of holes in the narrow wall of the waveguide [6]

LWAs can produce narrow beams, but the beamwidth is restricted by the structure's size. On the guiding structure of an LWA, the phase constant is less than the free-space wavenumber "k_0". As a result, the leaky wave is fundamentally a radiating type of wave, radiating or "leaking" power continuously as it propagates on the guiding structure, hence the name of the antenna. Because of the leakage of power, the propagation wavenumber, $k_z = \beta - j\alpha$ on the guiding structure is complex, consisting of both a phase constant *"β"* and an attenuation constant *"α"* (even if the structure is lossless). The phase constant (β) of the leaky wave controls the beam angle, while the attenuation constant (α) controls the beamwidth. To control the sidelobe level or the beam shape, the aperture distribution can be tapered. Using these fundamental design tricks, one can optimize the radiation and impedance performance of an LWA.

2.2 Classification of Leaky Wave Antenna (LWA)

LWAs can be classified into different categories, depending on the geometry and the principle of operation. The first distinction is between a one-dimensional (1D) leaky-wave antenna and a two-

dimensional (2D) leaky-wave antenna. A 1D leaky-wave antenna is one where the guiding structure is basically one dimensional; that is, the structure supports a wave traveling in a single fixed direction [13]. In the case of 2D leaky-wave antenna, the guiding structure consists of a two-dimensional surface and the leaky wave is a cylindrical leaky wave that propagates outward in the radial direction from the source [17], [18]. The focus of this work will be on 1D LWAs. Therefore, the discussion in this thesis is kept closely around this class of LWAs.

1D LWAs can be further divided into two types: uniform (or quasi-uniform) and periodic. As per the name, the uniform antenna structure has a consistent pattern that is distributed along the antenna length [19]. Such a design allows for the wave propagation in the fast region with its wave number defined as, $k_z = \beta - j\alpha$. The phase constant for the fast-wave propagation should be in the range $0 < \beta < k_0$. Practically, it may be difficult to realize a uniform LWA structure, therefore quasi-uniform LWAs are usually designed as they can be approximated as uniform LWAs [20]. In such a scenario, the structure is a periodic one that allows to maintain the condition on phase constant. Interestingly, the periodicity does not affect the radiation characteristics of the antenna directly. A periodic LWA can support both types of wave propagation i.e., fast and slow wave. In the latter case, the phase constant must meet the following condition $\beta > k_0$ [21] - [23]. By adding periodicity along the length of the structure, the fundamental propagating mode of the wave is made to radiate. Whether the wave is a fast or slow wave depends on the wavelength/frequency of the excitation signal. This will also determine the direction of radiation as will be discussed in the next section.

2.3 Physics of Leaky Wave Antenna (LWA)

The analytical model of LWAs must be studied in two steps. In the first case, the wave is propagating as a fast wave, i.e., $|\beta| < k_0$. Following up on this analysis, the slow wave propagation i.e., $|\beta| > k_0$ can be studied later. For this study, a simple case of an aperture with an electric field in the y-direction, as shown in Fig. 2.2, is selected. The electric field $E_y(x, y)$ on the aperture ($x = 0$) in the form of a leaky wave can be expressed as,

$$E_y(0, z) = Ae^{-jk_z z} \tag{2.1}$$

where complex wavenumber k_z ensuring propagation in z-direction is given by

$$k_z = \beta - j\alpha \tag{2.2}$$

also, β and α are the phase and attenuation constants respectively, while A is a coefficient expressing the maximum amplitude of the electric field. It is noteworthy to mention it here that 'α' in the case of a LWA defines the loss of power due to the leakage of the wave as it propagates along the length of the aperture. For practical purposes, this value of 'α' also includes the dielectric losses due to the substrate and the conductor losses due to the finite conductivity of the conductor. In many cases, the designers ignore the conductor losses as they are usually quite insignificant.

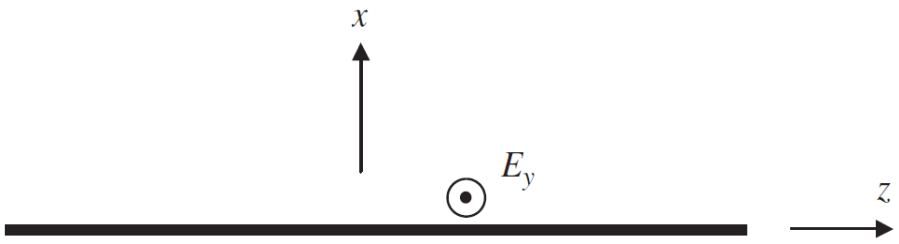

Fig. 2. 2: An infinite aperture showing radiation from a leaky wave with aperture at x =0 [6]

The radiated field above the aperture in the air (x > 0) can be written as

$$E_y(x,z) = Ae^{-jk_z z}e^{-jk_x x} \tag{2.3}$$

Importantly, the wave number in the *x*-direction 'k_x' of the radiated field is dependent on the wave number in the *z*-direction of the aperture 'k_z' as:

$$k_x = (k_0^2 - (k_z)^2)^{1/2} \tag{2.4}$$

where k_0 is free space wavenumber. Using $k_x = \beta_x - j\alpha_x$, squaring Eq. (2.4) and substituting the values of $k_x \; and \; k_z$ results in the following expression:

$$\beta\alpha = -\beta_x\alpha_x \tag{2.5}$$

Assuming that the wave is a forward wave with $\beta > 0$ and $\alpha > 0$ and is propagating in the $+x$ -direction away from the aperture, it follows from Eq. (2.5) that $\alpha_x < 0$. Strangely enough, this means that the wave in air is increasing exponentially, as opposed to decaying as it moves away from the source (aperture). This sounds unnatural and non-practical. In general, a radiating wave decays in amplitude as it moves away from the source. Thus, one can deduce that the fast wave in an LWA violates the basic principles of antenna radiation. However, this conundrum can be solved with help of a simple ray diagram shown in Fig. 2.3 [6].

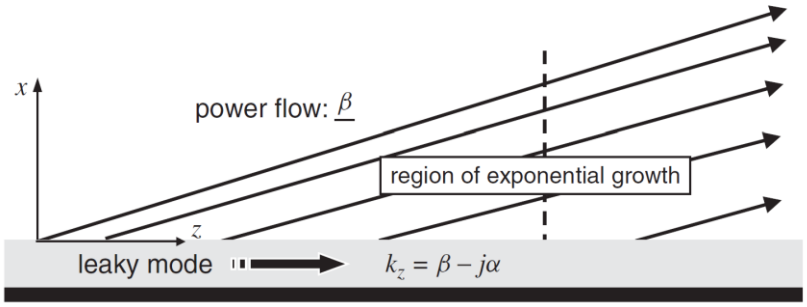

Fig. 2. 3: Ray picture for a forward leaky wave [6]

In Fig. 2.3, the power flow is depicted with the help of the rays that are leaving the top of the aperture with a phase constant, β. The leaky wave mode is moving in the z-direction along the substrate with a wave vector, k_z and phase constant, β_z. Using basic principles of geometry, one can write the following vector equation for β.

$$\boldsymbol{\beta} = \hat{\mathbf{x}}\beta_x + \hat{\mathbf{z}}\beta_z = \mathrm{Re}\,(\mathbf{k}) = \mathrm{Re}(\hat{\mathbf{x}}k_x + \hat{\mathbf{z}}k_z) \tag{2.6}$$

If θ_0 is the angle of the rays with respect to z-axis then it can be given by,

$$\tan\theta_0 = \frac{\beta_x}{\beta_z} \tag{2.7}$$

For small value of attenuation constant α, the angle θ_0 can be approximated as

$$\cos\theta_0 = \frac{\beta}{k_0} \tag{2.8}$$

This equation is used to measure the beam angle of the leaky wave antennas and is used by the designers to formulate their basic antenna structures. The separation of rays in Fig. 2.3, is dictated by the periodicity of the leaky wave structure and is directly responsible for the radiation intensity. Smaller the distance between these rays, the greater will be the strength of the radiated field and

vice versa. The ray diagram of Fig. 2.3 validates the mathematical formulation of Eq. (2.5) which states that the field level increases along the vertical line away from the aperture. Once the field maximizes in a particular direction, moving further higher in space will allow the intensity of field to decay. Thus, the physics of the LWA obeys the fundamental laws of physics. Also, it should be emphasized here that the total α is due to the leakage of the wave and the losses in air.

Now, one would like to study the radiation of a wave from a 'backward wave' also known as 'slow wave' as shown in Fig. 2.4, The figure implies that the phase and group velocities are opposite. As the wave in the substrate travels along $+z$ -direction, the radiated or leaked wave comes out of the aperture and propagates in the $-z$ -direction. Thus, the group velocity (normally the direction of power flow) is assumed to be in the $+z$ -direction, while the phase velocity is assumed to be in the $-z$ -direction, and therefore $\beta < 0$ in this case (slow wave). For this case, the wave field is propagating in the $+x$ -direction in air, therefore it is imperative that $\beta_x > 0$ to satisfy the physical principle of wave propagation. This results in, $\alpha_x > 0$ as can be seen from Eq. (2.5). In such a scenario, the leaky wave fields are 'proper' due to the decaying exponential characteristics in the direction of propagation. Due to this, the slow wave is known as the proper mode for a LWA. It should be kept it mind that while uniform LWAs can only support fast or forward propagating wave, the periodic LWAs are able to support both forward (fast) and backward (slow) propagating waves. Due to this property, the periodic LWA is of more interest for this thesis.

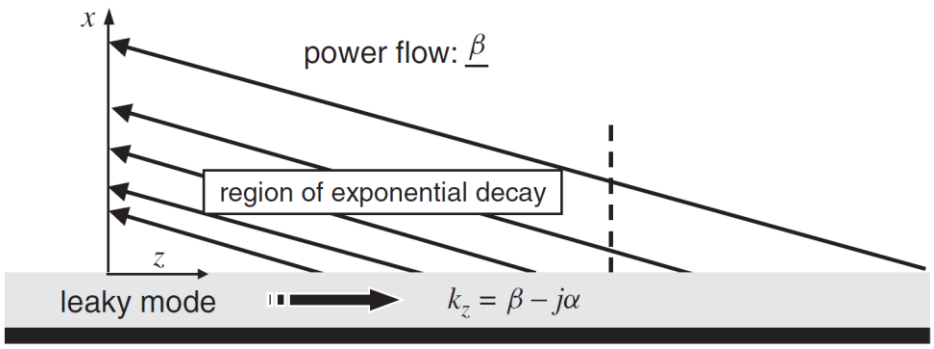

Fig. 2. 4: Ray picture for a backward leaky wave [6]

The analytical model of LWA, that has been discussed until this point considers an infinitely long antenna structure. However, in practice it is not possible to design an antenna whose length is infinite. One would like to study the antenna under finite considerations and with the feed point clearly identified. For this purpose, Fig. 2.5 shows the ray diagram of an LWA which is fed at $z = 0$ with the electric current and electric field propagating in both directions i.e., $z > 0$ and $z < 0$. For symmetricity/simplicity, one can assume that there is only forward/fast wave propagation and that the field propagating on either side is the same, i.e.,

$$E_y(0,z) = Ae^{-jk_z|z|} \tag{2.9}$$

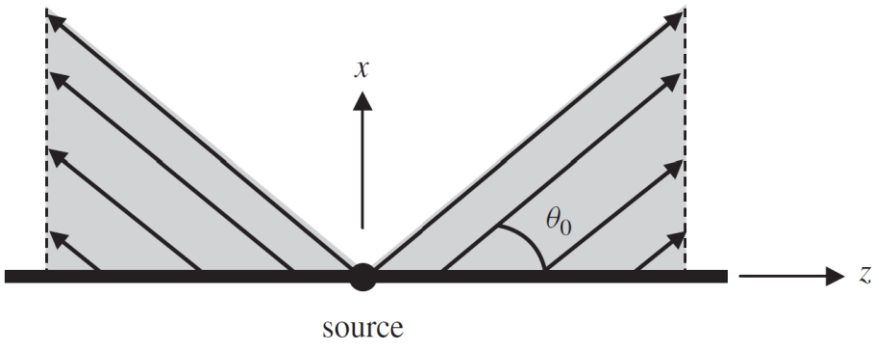

Fig. 2. 5: Ray diagram of a leaky wave excited by a line source at z=0 [6]

Since the image is symmetric around the vertical *x*-axis, the following discussion is limited to the area $z > 0$ for simplicity. Assuming that the antenna is radiating its maximum at $\theta = \theta_0$ in $z > 0$ direction while its mirror-reflection can be observed in the radiation along $z < 0$. The magnitude of the electric field is increasing until $\theta = \theta_0$, after which it decays in strength. Thus, the shaded area has the maximum radiation and the field within the shaded region defined by $\theta_0 < \theta < \pi/2$ is negligibly small. This boundary condition will allow the antenna to follow the basic principles of the LWA while upholding the fundamental principles of wave propagation, whereby the radiation should decay and approach to zero at infinity.

A simple Fourier transform method can be used to measure the exact field $E_y(x, z)$ due to the aperture field and is given in Eq. (2.10).

$$E_y(x,z) = \frac{1}{2\pi}\int_{-\infty}^{\infty} \tilde{E}_y(0,k_z')e^{-jk_x'x}e^{-jk_z'z}dk_z' \tag{2.10}$$

where the Fourier transform of the aperture field is

$$\tilde{E}_y(0,k_z') = A\left[\frac{2jk_z}{(k_z'^2 - (k_z)^2)}\right] \tag{2.11}$$

and vertical wavenumber is given by

$$k_x' = (k_0^2 - k_z'^2)^{1/2} \tag{2.12}$$

To satisfy the radiation condition at infinity, the vertical wavenumber in Eq. (2.12) is chosen as a positive real number or a negative imaginary number.

If one solves for the electric field for such a problem with the boundary conditions as defined here, then the radiation plot as shown in Fig. 2.6 can be achieved [6]. This is obtained by considering a special case where $\beta/k_0 = \sqrt{3}/2$ and $\alpha/k_0 = 0.02$. According to Eq. (2.8), this corresponds to a

leakage angle of $\theta_0 = 30°$. This is the point until which the magnitude of the electric field increases, after which i.e., $\theta > 30°$, a clear decay in the electric field magnitude can be observed.

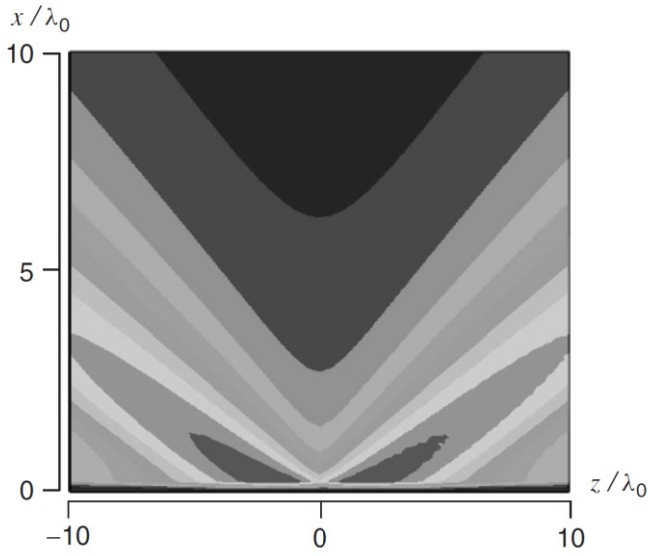

Fig. 2. 6: The magnitude of the electric field generated by a leaky wave on an aperture is represented as a contour plot. The parameters of the leaky wave are to $\beta/k_0=\sqrt{3}/2$ and $\alpha/k_0=0.02$ [6]

The same study can be carried out on a slow (backward) wave excitation. However, to avoid repetition, it is not included here since the two analyses are quite similar with the expected difference in the results [6].

2.4 Radiation Characteristic of One-Dimensional Leaky Wave Antenna.

In this section, the basic radiation characteristics of a LWA are described using a one-dimensional periodic leaky-wave antenna. It is noteworthy that the antenna is studied for its analytical model that is validated by experimental results [24]. The antenna consists of a rectangular waveguide with an important design modification. Instead of using metallic walls on all four sides of the antenna, the authors used grating of metallic strips on one of the walls along the waveguide length

while the other wall is completely metallized (Fig. 2.7). The top and bottom surfaces of the waveguide are completely metallic and are extended beyond the width of the guide. The length of this extension is defined as 'c', shown in Fig. 2.7. The extended parallel plate structure is defined as 'baffle'. It is not imperative for antenna radiation, but it can help to minimize the higher order modes from getting radiated. This will result in a pure linear polarization being radiated from the antenna aperture. In this case, the antenna has a finite length along z -axis, with the center of the antenna placed at $z = 0$. This means that the antenna extends in both direction from $z = 0$ in positive and negative z -directions. Let the total length of the antenna aperture be '$2l$', which implies that the antenna extends equally along the length (in z -direction) with a total dimension of 'l'. Now, for the antenna to radiate, a line source with current excitation is placed at (x_0, z_0). In a real-world scenario, this line source can be replaced with a coaxial feed. An important parameter here is the thickness of the substrate. This will dictate the scan angle at a particular center frequency.

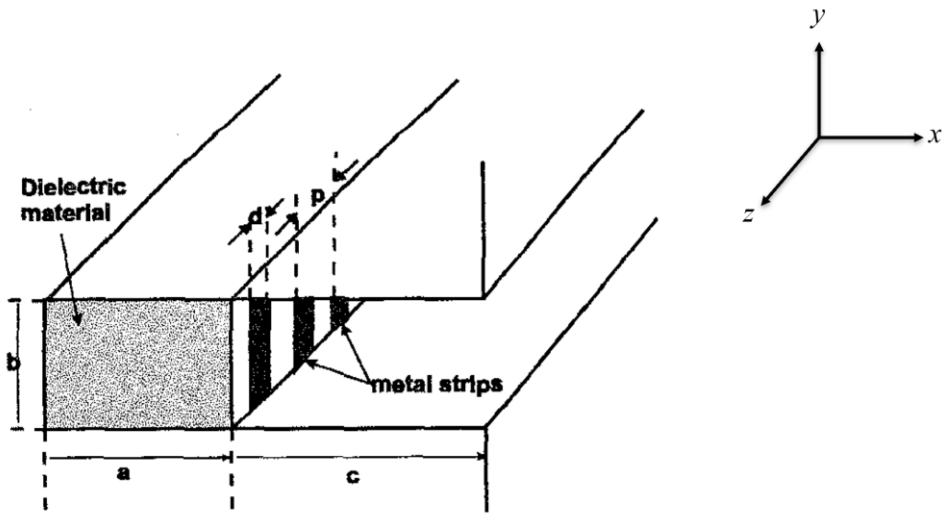

Fig. 2. 7: Leaky-wave antenna based on a metal-strip loaded dielectric waveguide [24]

The authors used Eq. (2.10) to solve for the radiation characteristics of the antenna. Applying the conditions of this antenna design on (2.10) results in the following normalized radiation pattern:

$$E_y^R(\theta) = cos\theta \int_{-l}^{l} E_y(c,z) e^{jk_z z} dz \tag{2.13}$$

where $k_z = k_0 sin\theta$.

The radiated field shown in Eq (2.13) can be used as a starting point for the design of an LWA. One would like to use this equation when starting the design of an LWA. The same step is performed by the authors in [24] to propose a different LWA structure. Designing an antenna on a low dielectric constant ($\varepsilon_r = 2.08$) substrate and targeting a center frequency of 7.49 GHz, the authors fabricated a waveguide based LWA to validate their mathematical model. With several results reported in the manuscript, here it is important to focus on the radiation pattern at 8.55 GHz. The rationale for choosing this frequency is that this is the only operating frequency where a comparison between the measured and calculated data is provided. An excellent match can be observed at 8.55 GHz in Fig. 2.8. The measured data is not as smooth as one would anticipate but that is due to the surface wave and space wave diffraction and can be reduced by controlling the total length '*c*'. By proper inspection and design optimization, these ripples in the measured data can be reduced significantly. Also, the front-to-back ratio can be further improved by improving the matching conditions. However, this is not of a major concern since the back lobe radiation is already several dBs less than the main lobe radiation.

Nonetheless, the authors in [24], for the first time presented a theoretical model for a practical LWA design, which is validated by the measurements.

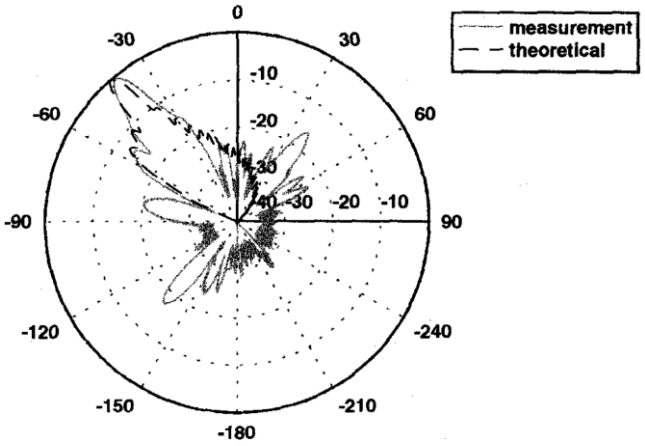

Fig. 2. 8: Theoretical and experimental radiation patterns at 8.55 GHz [24]

2.5 Reconfigurability of Leaky Wave Antenna

LWAs, as previously mentioned, have inherent frequency-based beam-scanning properties. In most cases, a wide frequency sweeping range is required for beam scanning. This frequency-dependent beam scanning technique may be useful in certain applications, such as frequency-scanning radars [25]. However, frequency-dependent beam scanning is unlikely to be used in many of the modern wireless communication systems such as Wi-Fi, Bluetooth, 5G, LTE etc. The main explanation for this is that most wireless communication systems use a predefined frequency band. With one dimensional LWA, this issue can be solved by electronically reconfiguring the leaky-line boundary condition. Using active devices such as varactor diodes or micro-electromechanical system (MEMS), the leaky mode complex propagation constant can be altered, thus producing the desired control of the scanning beam with fixed frequency. This thesis work focuses primarily on the radiation pattern reconfigurability for LWAs at a fixed center frequency.

2.6 Examples of LWA in Literature

Most of the LWA design in literature focus on beam scanning that is dispersive, meaning frequency dependent. Before delving into actual antenna design for this thesis, it is important to establish the state-of-the-art that exists in the field of LWA design. For this purpose, this section starts with the discussion of frequency dependent LWA that leads into the designs that present beam scanning at a single frequency.

2.6.1 Frequency Reconfigurable LWA

Classically LWAs have been used for beam steering applications by varying the frequency of the input signal. In terms of existing literature, this is where the discussion should begin. Usually, LWAs have been implemented using waveguides, however there has been a growing interest in using this antenna type with microstrip line as the feeding and radiation source. Microstrip leaky wave antennas (MLWA) are appealing because of their planar low profile, ease of fabrication, high efficiency, large bandwidth, and beam-scanning capabilities. An excellent example of microstrip based LWA is implemented and reported in [3]. The discontinuities in the antenna structure are provided with the help of via walls at the two lateral edges (Fig. 2.9(a)). These vias provide the required impedance change that result in the radiation of the traveling wave. The antenna radiates almost equally in two different directions as shown in Fig. 2.9(b). By sweeping the input frequency, the authors showed that both the beams of the antenna can be steered, and their radiating angles can be controlled. A simple analysis to understand the excitation of leaky wave modes is also presented in the paper that helps the readers to understand the working principle of the proposed antenna. The measured impedance of the antenna shows an impedance bandwidth of 23% that allows for an increased range of frequency sweeping, resulting in an increased beam

scanning range. While varying the frequency from 6.92 to 8.75 GHz the two antenna beams can steer in the following range of $(\theta; \pm\phi)$, $(75°; \pm 48°)$ to $(38°; \pm 60°)$. A maximum measured gain of 12.7 dBi is achieved with a variation of less than 3 dB throughout the frequency band.

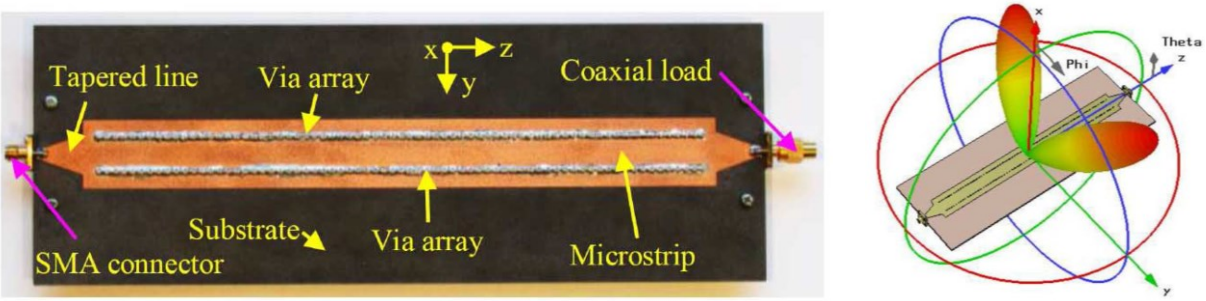

(a) (b)

Fig. 2. 9: Dual beam microstrip LWA. (a) Fabricated antenna prototype. (b) 3-D radiation pattern [3]

Like [3], another microstrip based LWA is proposed in IEEE Antenna and Wireless Propagation Letters (AWPL) in 2020. An even-mode-excited LWA loaded with elliptical annular ring patches is proposed in [7], as shown in Fig. 2.10. The rings along the microstrip line provide the proper impedance modulation while the vias are integrated on the edges of these rings to provide wide band impedance matching. While modifying the position of the shorting pins, the paper shows how one can control the propagation constant of the traveling wave which in turn helps to direct the beam in a particular direction. In addition, it also helps to optimize the gain of the radiated waves. The antenna radiates with its maximum in bore-sight direction when fed with a frequency of 14.8 GHz. While tuning the frequency from 10.7 to 17 GHz, a beam steering of 105° is measured while

maintaining a stable gain of 16 dBi. These results demonstrate the efficacy of the proposed microstrip LWA and outlines a simple design that can provide stable beam scanning results.

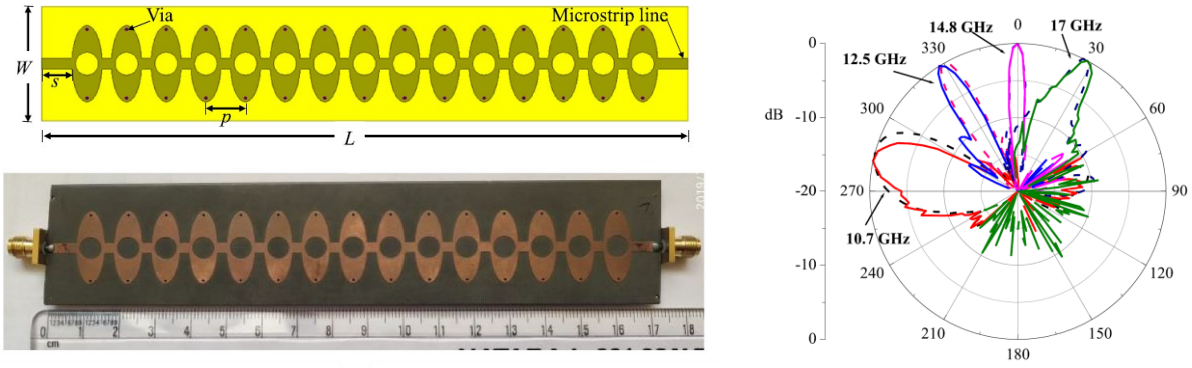

(a) (b)

Fig. 2. 10: (a) Proposed and Fabricated antenna prototype (b) Normalized simulated (dash line) and measured (solid lines) radiation patterns [7]

Similar to [3] and [7], Sarkar, *et. al.*, presented another variant of MLWA for wideband operation, Fig. 2.11(a) [26]. The antenna is designed to operate in V-band i.e., 50-65 GHz of the frequency spectrum. Scaling the center frequency at this band introduces more challenges due to the small wavelength of the signal. The antenna is this case is also designed to radiate in two directions as in [3] and therefore it is regarded as a dual-beam MLWA. The architecture uses a dominant-mode microstrip–slot line transformation to achieve forward beam scanning with symmetrical dual side pencil beam. By integrating PIN diodes on the structure in tandem with metallic vias, a virtual magnetic wall is created at the centre of the microstrip line. This magnetic wall causes the radiation from the microstrip line with forward scanning capability as shown in Fig. 2.11(b). With the help of dispersion plots, the authors analyzed the wave modes that are radiated out of the antenna

structure. An impedance bandwidth of 29.2% (52.5–65 GHz) is observed in measurements with a scanning range in H-plane of −65° to +69.7°. The maximum gain of the antenna remains stable at around 18 dBi with a minor variation of 0.7 dB when the diodes are biased. This is a rather unique design because of its high frequency operation and the introduction of a magnetic wall boundary in the antenna structure.

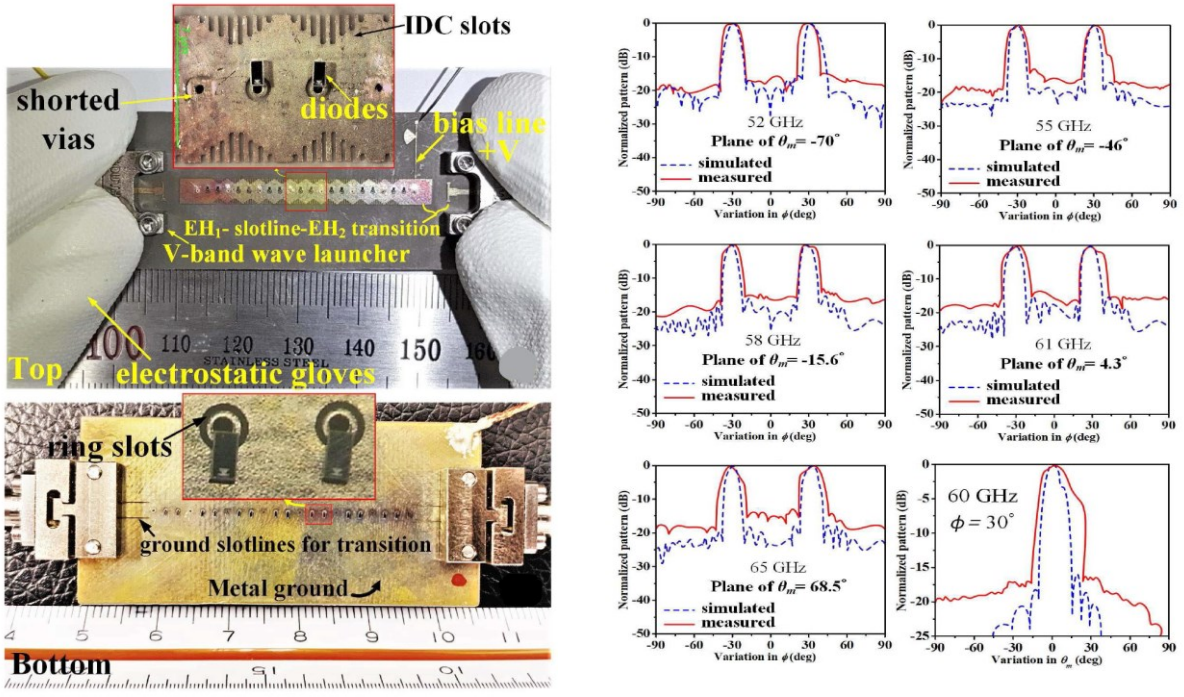

(a) (b)

Fig. 2. 11: (a) Proposed fabricated prototype (b) Simulated and measured normalized radiation patterns [26]

Further to the work that has been reported until this point a few other designs using MLWA structure have been reported very recently in literature [27]-[29]. Using line meandering [27], Yagi structure [28] and slot array [29], all these examples provide an effective design methodology that

can be employed to provide beam steering in various applications. With center frequencies of 10.8 GHz, 5.4 GHz, and 18 GHz, respectively it is shown that this class of antenna can be applied in different frequency bands and wireless applications as needed. Beam scanning of almost 90° can be seen from these designs, however, they do rely on variation of input frequency to steer the antenna radiation. The maximum gain in all these cases remains stable with variations of 3 dB in general. The viability of LWAs using microstrip feed lines is further validated by these examples due to the spectrum of the frequency bands that have been reported in these articles.

Lastly, in this section of frequency reconfigurable LWA, it is noteworthy to add one more design that can be defined as an MLWA. An improved half-width microstrip LWA with periodic short circuits shown in Fig. 2.12 is an intriguing design [30].

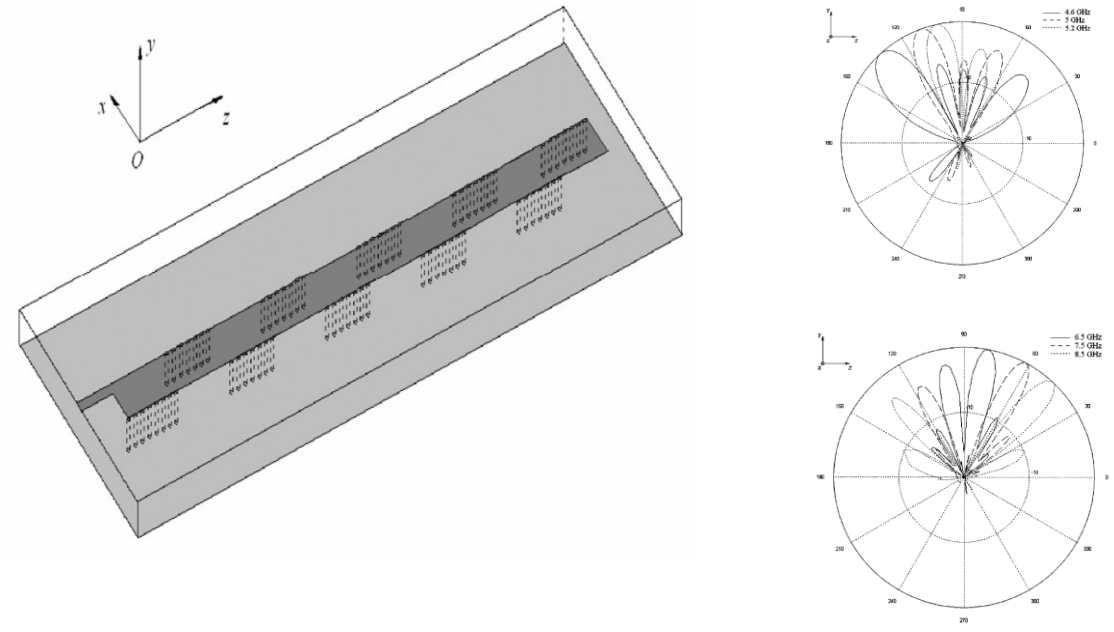

(a) (b)

Fig. 2. 12: (a) Microstrip LWA (b) Radiation patterns of the microstrip LWA [30]

The proposed antenna is composed of rectangular patch/feed with vias integrated at the lateral edges periodically. The vias do not form a continuous wall as has been seen in one of the designs before, rather they are spread equidistantly on either side. A repetitive pattern can be clearly seen in the structure. This simple periodic construction produces backward-to-forward beam-scanning radiation patterns (Fig. 2.12(b)). When the operating frequency is altered from 4.6 GHz to 8.5 GHz, the antenna's maximum radiation scans from 144° to 41° in the H-plane (*x-y* plane). As the antenna steers its beam, the side lobe levels can be seen increasing which is expected in such antenna elements. However, the radiation levels of the side lobes are kept in check, which in turn helps to maintain the maximum gain of the antenna. This is another example of MLWA and is the one, which is to be further studied in this thesis to present a novel LWA structure.

To summarize the literature of frequency dependent LWA, Table 2-1 is presented here. With a quick glance, the reader can have an idea of this particular type of antenna especially implemented using microstrip line.

Table 2. 1 Performance comparison of frequency sweep reconfigurable LWA

Reference	Venue	Frequency **[GHz]**	Beam Steering **[Degree]**	Gain **[dBi]**	Size **(Length x Width) [mm²]**	**Year**
[3]	IEEE TAP*	6.92 - 8.75	27°	12.7	254 x 90	2016
[7]	IEEE AWPL*	10.7 - 18	105°	16	170 x 30	2020
[26]	IEEE TAP*	52 - 65	135°	18.7	55 x 30	2020
[27]	IEEE APSIC*	10 - 10.5	30°	7	230 x 170	1996
[28]	IEEE AWPL*	4.9 - 5.6	78°	6.1	100 x 60	2018
[29]	IEEE TAP*	16.7 - 19.8	80°	17.4	170 x 30	2021
[30]	IEEE TAP*	4.6 - 8.5	103°	9	200 x 50	2011

TAP* ~ IEEE Transactions on Antennas and Propagation
AWPL* ~ IEEE Antennas and Wireless Propagation Letters
EuCAP* ~ IEEE European Conference on Antennas and Propagation
APSIC* ~ IEEE Antennas and Propagation Society International Symposium

2.6.2 Fixed Frequency LWA

One of the main disadvantages of the classical leaky wave antennas is that the radiation beam typically scans with the operating frequency. This is often problematic for many modern wireless applications, which require a fixed center frequency when the antenna beam is scanned. It has been shown in some literature that the maximum antenna radiation of LWA can be steered at a single frequency [4]. Such designs are more applicable to conventional modern day communication systems. Here, the focus is on MLWA designs that can provide the stated antenna performance. A technique that has been implemented to achieve fixed-frequency beam scanning from MLWAs is by using half-width MLWA (HW-MLWA) configuration [4]. A long microstrip line with low impedance is loaded with vias and with the help of integrated switching elements as shown in Fig. 2.13(a) [4]. The authors use binary switches to either connect the via to the line or disconnect it. The loading structure can be regarded as a unit cell that can be reconfigured between two extremes. A macrocell is formed by combining multiple reconfigurable unit cells, and the periodic LWA is formed by cascading identical macrocells. To validate the concept, a prototype HW-MLWA is designed, developed, and realized. The end of the line is terminated with a matched load to prevent any unwanted reflections. The antenna is measured using a switching element and a p-i-n diode. The results at 6 GHz are illustrated in Fig. 2.13(b). CBP stands for complete binary pattern, which describes the binary pattern of any macro cell state in terms of 1's or 0's, and each macro cell is made up of *M* unit cells, as shown in the table of Fig.2.13(b). The main beam scans between 31° and 60° from the bore-sight direction. The measured peak gain of the antenna is 12.9 dBi at 6 GHz, and with a gain variation of 1.2 dB.

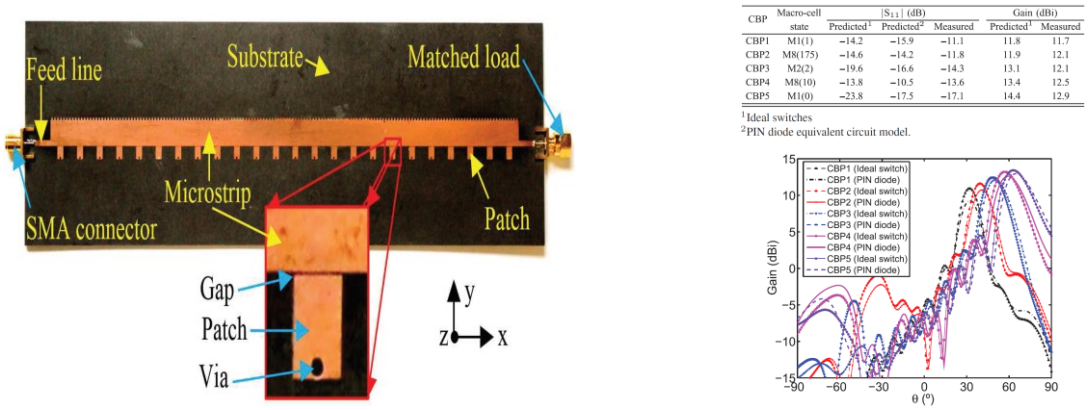

CBP	Macro-cell state	$\|S_{11}\|$ (dB)			Gain (dBi)	
		Predicted[1]	Predicted[2]	Measured	Predicted[1]	Measured
CBP1	M1(1)	−14.2	−15.9	−11.1	11.8	11.7
CBP2	M8(175)	−14.6	−14.2	−11.8	11.9	12.1
CBP3	M2(2)	−19.6	−16.6	−14.3	13.1	12.1
CBP4	M8(10)	−13.8	−10.5	−13.6	13.4	12.5
CBP5	M1(0)	−23.8	−17.5	−17.1	14.4	12.9

[1] Ideal switches
[2] PIN diode equivalent circuit model.

(a) (b)

Fig. 2. 13: (a) Fabricated antenna prototype (b) Radiation pattern with respect to macro-cell state [4]

Like [4], Y. Li, *et. al.*,[31] presented another MLWA design which relies on off-the-shelf switch component, Fig. 2.14(a). The antenna system consists of a microstrip patch and two feeding terminals. The MLWA is excited using two ports that can be broadly labelled as *A* and *B*. The positions of ports *A* and *B* can be varied along the length of the antenna to control the direction of main lobe. To illustrate this, the authors used 3 different excitation points for port *A* and identified them as port 1, port 2, port 3, while for port *B* the nomenclature of three positions is regarded as port 1′, port 2′, port 3′ respectively. The programmable switch is used to control the various feeding terminal combinations along the side of the MLWA, allowing the main lobe to scan at both sides progressively. At 7 GHz, the measured results show that the antenna provides a dual-beam radiation that can be steered using this method. By manipulating the feeding configuration, the design proposes beam scanning at a single frequency while providing acceptable impedance and radiation performance. The two main beams scan from 41.16° to 63.01° and from 116.75° to 138.59° as depicted in Fig. 2.14(b).

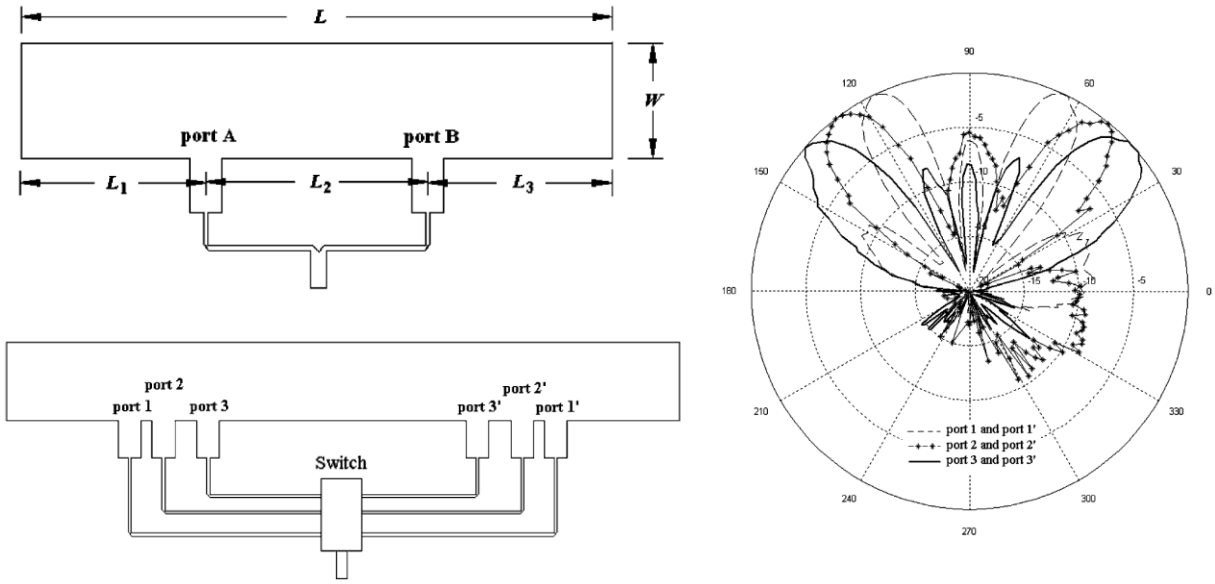

(a) (b)

Fig. 2. 14: (a) Layout of MLWA (b) The radiation patterns of MLWA fed by three different feeding terminal combinations [31]

A last example of the antenna type under discussion (MLWA) is published in 2017 by authors from Indian Institute of Technology [32]. Using varactor diode loading, the antenna can steer its beam when the capacitance is configured to different values. Due to the low frequency of operation, the antenna's size is reasonably large (200 mm). However, it is expected that further increasing the length of the antenna will not only improve the antenna gain but also provide better steering range. Having written that, the authors kept in view the practical constraints when designing and implementing this antenna. The microstrip comb-line reported in [32] is diagrammatically represented in Fig. 2.15. With increasing bias voltage across the varactor diode, the antenna achieves 4° to 46° backward beam scanning with respect to bore-sight. A maximum

gain of 7.7 dBi is measured from the antenna with acceptable variation of 2.3 dB while scanning the beam.

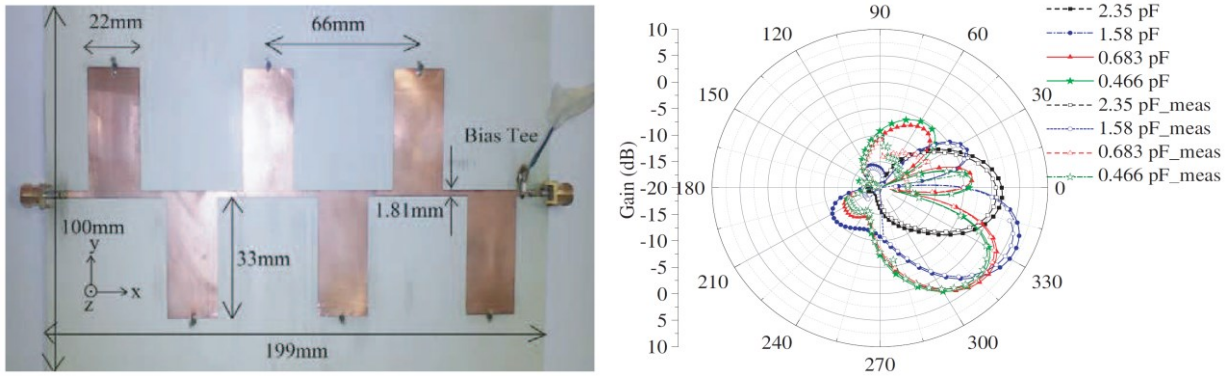

(a) (b)

Fig. 2. 15: (a) Photo of fabricated antenna (b) Simulated and measured realized gain patterns at 2.4 GHz for different bias voltages of varactor [32]

2.7 Conclusion

This chapter starts with the basic theory of the LWA antenna design to provide an understanding about the radiation characteristics of the antenna. The brief description of LWA's fundamentals is followed by a comprehensive literature review on different types of MLWA antenna. Since the focus of this thesis is on microstrip based antenna designs, the literature review has been kept focussed around this topic. As per the chronology of LWA, the designs that show beam scanning capabilities by varying the input signal frequency are initially discussed. Most of the work in the field of LWA design reports beam scanning in this manner. This type of design requires large impedance bandwidth to show proper operation. A summary table of MLWA designs that rely on frequency-based beam steering is included in the chapter. At the conclusion of the chapter, it is

demonstrated that little research has been conducted on LWA designs that achieve beam scanning at a single operating frequency. Although there are some designs reported in the literature, it is believed that this area can be further explored for research to propose designs that can find applications in modern communication systems. Thus, the author in this work plans to explore a novel reconfigurable technology known as FPMS for the design of a single frequency beam-steerable LWA. Such a design will be able to do-away with the dispersive properties of the LWA design while providing the required beam steerability.

Chapter 3

Field Programmable Microwave Substrate (FPMS)

The second chapter of this thesis delves into the specifics of the LWA design, beginning with the fundamental theory and progressing to a description of the current state-of-the-art in this field. One basic conclusion that is drawn at the end of the last chapter is scarcity of fixed frequency LWA design. Therefore, the central interest of this thesis is to come up with a reconfigurable LWA design that can provide beam steering at a single center frequency. Now when it comes to microwave applications, tunable and reconfigurable microwave circuits have almost reached saturation. A variety of techniques such as lumped-element loading [33], magnetic materials [34], ferroelectric components [35] etc. have been explored to achieve the desired results of reconfigurability.

However, a novel idea that has been proposed in 2016 by N. Jess [36], known as field-programmable microwave substrate (FPMS) is mostly untouched when it comes to antenna design. Even the very first publication on this topic relied on demonstration of circuits, based on a novel programmable microwave waveguide [36]. The paper has shown that an FPMS based waveguide that has the ability to reconfigure the substrate properties without replacing any physical components. Using this concept, the authors extended the work to show a working tunable filter, controllable oscillator and a frequency tuned amplifier. The reconfigurable waveguide thus presented shows an unprecedented level of programmability. The use of FPMS in the RF domain is analogous to the use of a field-programmable gate array (FPGA) in the digital domain, thus the nomenclature.

In this chapter the fundamentals of FPMS are discussed by introducing its unit cell design and their implementation. After providing a brief over-view of [36], it shown that how the FPMS unit cell is optimized for the LWA design with respect to its dimensions and capacitive values. All simulations were run on a Duroid 5880 substrate with a center frequency of 2 GHz, and the findings are summarized here.

3.1 Field Programmable Microwave Substrate

The operation of FPMS can be understood by first explaining its building block known as a 'unit cell, and then describing how it is implemented to demonstrate its capabilities as a programmable waveguide [36].

3.1.1 FPMS Unit Cell

The small unit cells used in realization of FPMS can be individually reconfigured to have a range of positive or negative dielectric constants. It consists of two microstrip lines that are connected to each other perpendicularly. The intersection of the lines is loaded with a varactor diode that functions as a variable capacitor and biased with the help of an RF choke resistor, '$R1$'. A capacitor '$C1$' act as a DC blocker and is connected in parallel with this resistor to provide RF path to the ground. The unit cell design is pictorially shown in Fig. 3.1. FR4 substrate is used for the implementation of this structure. In simulations, the authors of [36] used a dielectric constant of 4.9 and a dielectric loss tangent of 0.015-0.02. Each unit cell consists of metallization (brown in color), varactor "$V1$", resistance "$R1$" of $10k\Omega$, decoupling capacitor "$C1$" of value 2.2 nF. Since the metallization includes both the direct-current (DC) and radio-frequency (RF) signals, resistance $R1$ and capacitance $C1$ are integral for the implementation of this structure. The optimized unit cell design has dimensions of W = 0.5 mm and L' = 2.54 mm, resulting in a total

structural dimensions of 5.08 mm x 5.08 mm for the plus shape metallization. The thickness of the substrate as used for this design is 1.17 mm.

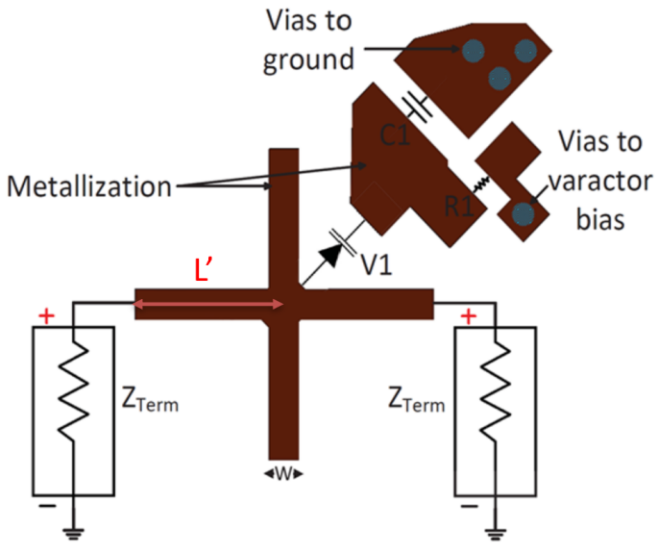

Fig. 3. 1: Unit cell used to construct FPMS [36]

The unit cell metal structure of Fig. 3.1 is simulated using Keysight's Advance Design System (ADS) in Momentum (layout), and in co-simulation (EM and circuit simulation combined). The S-parameters of the structure can be used to extract the material properties experienced by the wave using Nicolson-Ross-Weir (NRW) method [37]. NRW is a well-known algorithm that has been classically used to extract material properties of a substrate from its impedance parameters. In RF theory, this is a fundamental technique and therefore it is not discussed in detail in this thesis. Nevertheless, the effective material properties for different bias on the varactor is studied. The properties shown in Fig. 3.2 show that the effective dielectric constant of the unit cell can be modified by varying the bias on the varactor diode. At 1 GHz, the dielectric constant value ranges from 7 to 13 when the bias is varied from 25 V to 8 V. The rationale for focussing on 1 GHz here

is because 2 GHz is either very close to resonance here or it is the resonant point. Because this is the first-ever implementation of the FPMS technology, 1 GHz was rightly chosen due to the limitations of the FR-4 substrate, which only works well until 4 GHz, and also to keep the design simple. It is also important to mention it here that the dielectric properties of the material at a particular bias remains constant until a maximum frequency known as resonance frequency. This resonant point exists due to the capacitor's own resonance behavior. That is to say that, when the capacitor reaches its self-resonance, it will start behaving as an inductor. As a result, the wave experiences a negative permittivity since the reactance is now inverted. Hence, the presence of self-resonant point. Further, it can be noted from Fig. 3.2, that the value of self-resonance changes as the varactor bias voltage changes. These characteristics are critical as they will ascertain the frequency bandwidth of the design in which it can be tuned or reconfigured.

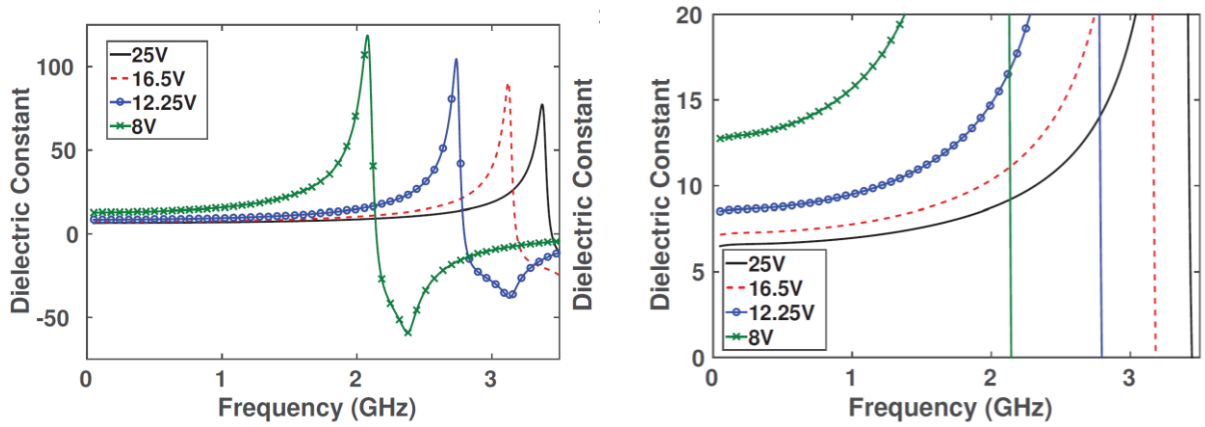

Fig. 3. 2: (a) Effective dielectric constant of unit cell (b) The magnified version [36]

In addition to dielectric constant, it is interesting to study the loss behavior of the proposed substrate. For this purpose, loss tangent in also plotted alongside dielectric constant, shown in Fig. 3.3. The resonance frequency in this case is similar to the ones reported in Fig. 3.2. The loss tangent values are in the range of 0.01-0.02, which makes sense. The rationale for this conclusion is the inherent loss tangent of FR-4 substrate. Thus, a lower loss substrate can result in better loss performance of the unit cell structure and is worth exploring.

To complete the loop on this circuit, the magnetic properties of the unit cell are also plotted/extracted in Fig. 3.4. Generally, it is anticipated that the relative magnetic constant of a substrate should be equal to 1. In this case, it is slightly greater than 1 due to the increased series inductance from the metal cross structure employed in the unit cell design. The magnetic constant in Fig. 3.4 is greater than unity. This property is also reflected in Fig. 3.5, where the magnetic loss tangent of the material is drawn. In an ideal scenario (substrate), the magnetic loss of the material should be zero. The non-zero value in this case can be attributed to the conductor loss incurred due to the metal structure. Adding the magnetic and dielectric loss tangents, results in overall power loss that a wave experiences when traveling through a medium.

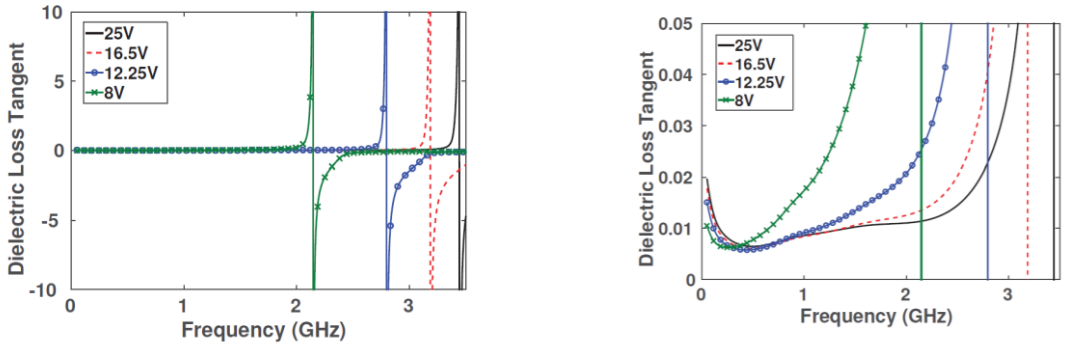

(a) (b)

Fig. 3. 3: (a) Effective dielectric loss tangent of unit cell (b) The magnified version of (a) [36]

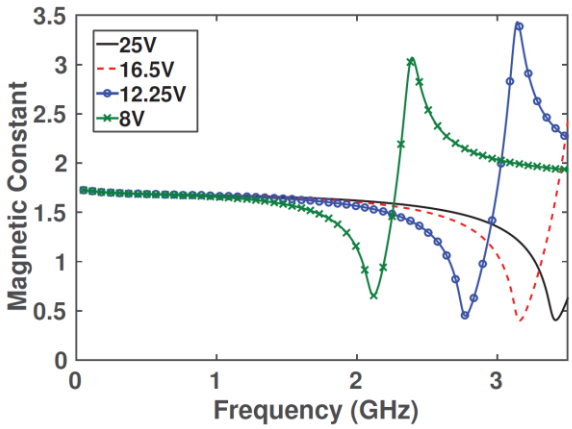

Fig. 3. 4: Effective magnetic constant of unit cell [36]

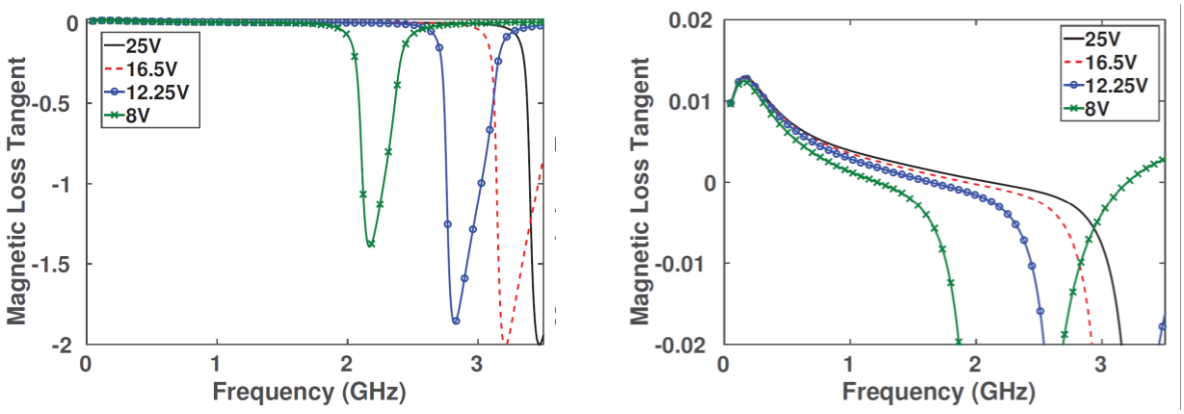

(a) (b)

Fig. 3. 5: (a) Effective magnetic loss tangent of unit cell (b) The magnified version of (a) [36]

3.1.2 FPMS Implementation

With the introduction and study of the basic building block of the FPMS technology i.e., unit cell, the next logical step is to apply its implementation in actual PCB board and analyze its efficacy for the realization of fundamental RF/microwave components. To accomplish this, Nathan et. al.

[36] designed and fabricated a 16x16 elements based FPMS demonstration board on FR-4 substrate. The board consist of three microwave ports, a transistor in common emitter configuration, an inductor (circle in red) that grounds the anode of the varactor, and two capacitors (circle in blue) of capacitance 3pF attached to it to block DC and filter out low frequency signal. The complete proof-of-concept design is shown in Fig. 3.6(a) with a magnified version of the unit cells shown in Fig. 3.6(b).

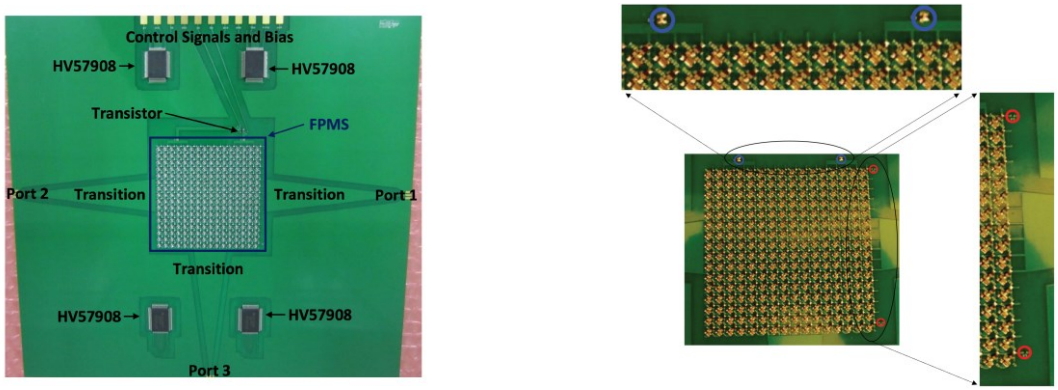

(a) (b)

Fig. 3. 6: (a) Implementation of FPMS on FR4 (b) Close-up picture of an FPMS with 256-unit cells [36]

To validate the integration of multiple functions on a single board, RF functions such as waveguide-based filters, oscillators and amplifiers are all simulated and measured. This level of versatility is particularly unique to the FPMS technology and highlights its novelty. With the help of the dynamic control that the FPMS unit cells provide to the designers, it is demonstrated in [36] that the waveguide can be tuned for its center frequency as well as impedance bandwidth. Similarly, the oscillator and amplifier functions are shown to be completely controllable by tuning the center frequency of these designs by the virtue of the FPMS unit cells. To keep this discussion

concise, only the results of waveguides are shared in this chapter. The design representation is illustrated in Fig. 3.7 where each square block is realized using the FPMS unit cells. These unit cells can be biased at different varactor voltages to control the dielectric properties experienced by the wave. In Fig. 3.7, the white colored blocks are biased to provide a negative dielectric constant while the blue colored blocks provide the positive dielectric constant for the propagating wave. As a result, the wave only passes through the blue region while avoiding the white one altogether. By selecting different number of blue cells along the width, one can control the center frequency of the waveguide. Thus, the three waveguides with different widths show different frequency response as can be seen in Fig. 3.8. With not much change in the insertion loss, the impedance bandwidth and the frequency can be tuned as per the requirements. Furthermore, it is shown that the ON-voltage for the varactor can also be varied to provide another degree of freedom. Therefore, 25 V as well 10.7 V are both used in the test set up with minimum effect on the overall performance.

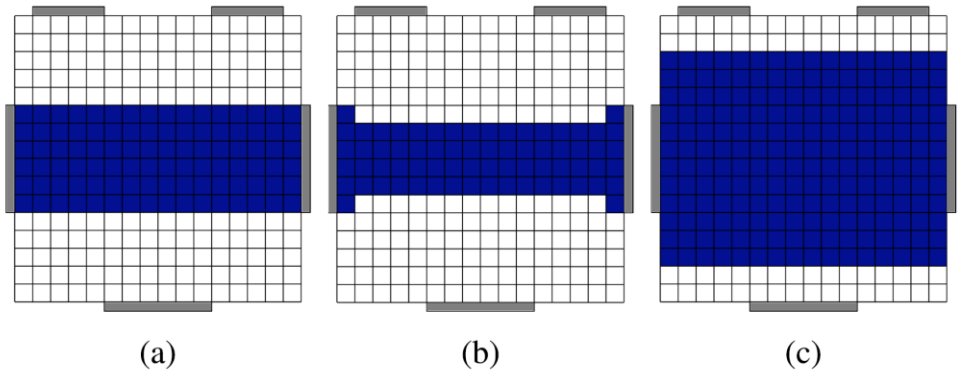

Fig. 3. 7: FPMS implementation for waveguide (a) Bias = 25 V. (b) Bias = 25 V. (c) Bias = 10.72 V [36]

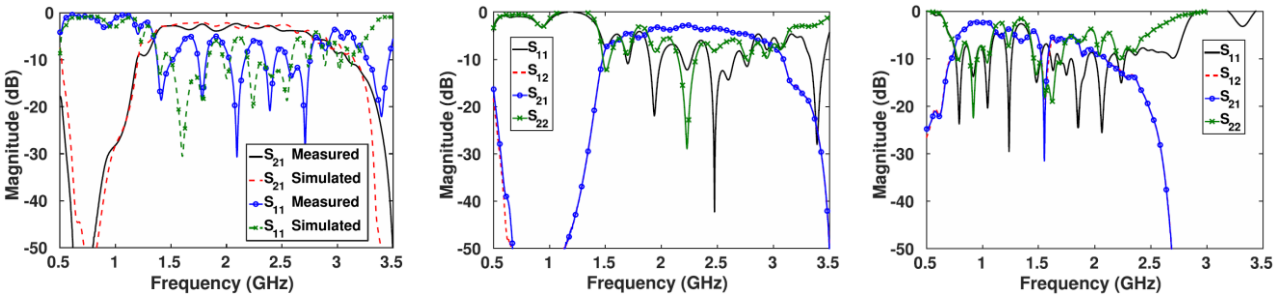

(a) (b) (c)

Fig. 3. 8: FPMS implementation for waveguide (a) Bias = 25 V. (b) Bias = 25 V. (c) Bias = 10.72 V [36]

3.2 FPMS Unit Cell Optimization for 2GHz

To design an antenna using FPMS unit cells, it is important to first understand the operating principle of these unit cells with the help of a Full-wave simulator like Ansys High Frequency Structure Simulator (HFSS). The previous work on FPMS relied on a circuit simulator i.e., Keysight's ADS to demonstrate its RF performance. However, for an antenna design, the same software cannot be used because of its inherent limitations. Therefore, in this work, all the simulations are to be carried out using HFSS. FPMS has never been used for antenna and wave simulations. Thus, this is the first ever attempt to integrate this technology into a radiating structure.

For now, the design frequency is kept at 2 GHz to reduce the number of unknown variables. The substrate used in [36] is FR-4 which is quite lossy when it comes to RF frequencies. The loss tangent of FR-4 is 0.015-0.02 which is clearly not the best. Also, for antenna designs, it is deemed that the dielectric constant of the substrate should be as low as possible to provide higher gain values. Keeping this in view, Duroid 5880 substrate is chosen for the antenna and the unit cells

designs studied on this platform. One final selection is that of the varactor diode. Skyworks SMV 1242 is a good candidate as it operates up to 10 GHz with reasonably low loss. The datasheet of the varactor is available from the manufacturer and provides the equivalent circuit values that can be employed to model this diode/varactor. Throughout this work, all the simulations are completed using this varactor at different bias values (different capacitance values). Several steps are taken to optimize the dimensions of the unit cell, substrate parameters and capacitance values of the varactor. All these variations are studied in detail and their discussion is covered in the upcoming sections.

3.2.1 Substrate Material

When starting the design simulations, it is better to use the exact same structure as used by Nathan et. al. [36] to demonstrate the first simulation results on Duroid. This will help to better understand the simulated results. The major difference here is that Duroid 5880 is used as a substrate in this case. Duroid 5880 has a dielectric constant of 2.2 and a loss tangent of 0.0009. The reflection coefficient along with its dielectric constant of the unit cell with Duroid 5880 substate material is shown in Fig. 3.9 for the same structure as reported in [36]. The S-parameter results shown here are quite expected. The results represent matched conditions until the varactor reaches its resonance where the capacitance starts behaving as an inductor. After which the power is reflected back to the input as is shown in the simulated results. Nonetheless, using these S-parameters the extracted properties of the substrate are also plotted. Here again, the negative permittivity of the substrate explains the reason of power getting reflected back. In a nut-shell the results show the starting point from where the unit cell can be studied for different design parameters.

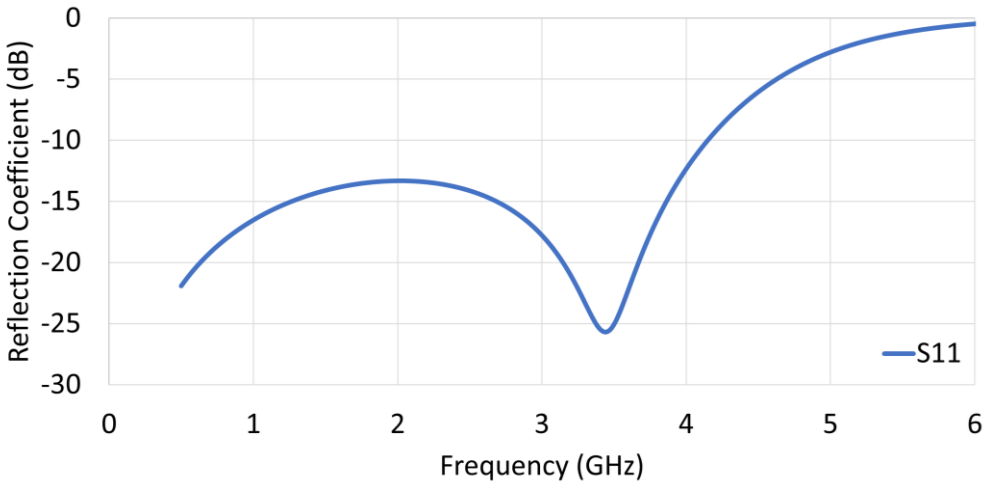

(a)

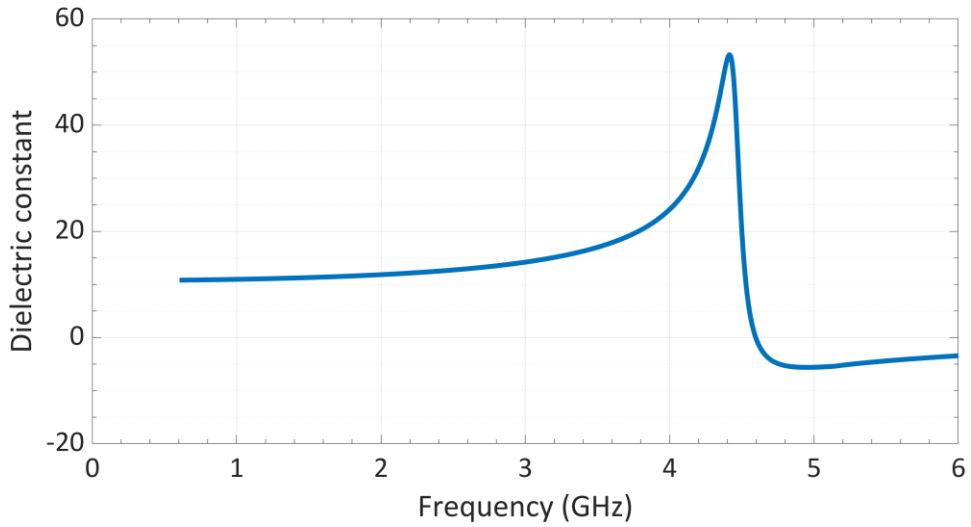

(b)

Fig. 3. 9: (a) Reflection Coefficient of unit cell with Duroid 5880 (b) Dielectric constant

3.2.2 Unit Cell Optimization with respect to Line Dimensions and Substrate Thickness

At first, the unit cell optimization is to be carried out by varying the length (*L*) of the metallization (orange color) and the thickness *(T)* of the substrate, as shown in Fig. 3.10. The primary goal of this optimization is to investigate all possible options for the unit cell size and the effect of substrate thickness on its impedance performance. The unit cell size should be realistic for practical implementation as well as in terms of its frequency response. The width *'W'* of the metal is kept constant at 0.5 mm since this does not play a key role in optimizing the cell performance. The two metal lines of the unit cell metallization have equal lengths '*L*'. The point of intersection of the two lines is where the varactor (capacitor) is integrated, as shown in Fig. 3.10. Since these are early simulations, a fixed capacitor value (1 pF) has been integrated into the unit cell design. This allows one to isolate the effect of the capacitor loading from the basic structure. Thus, the reason for this choice of simulations.

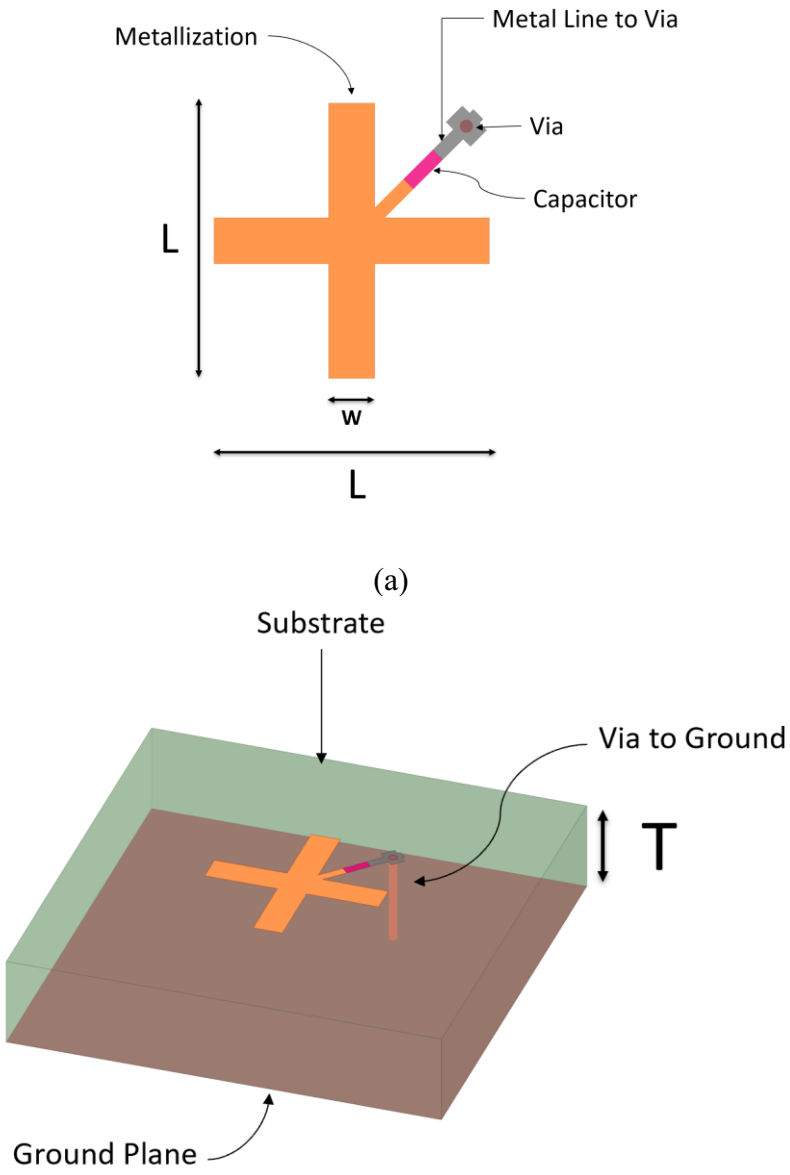

Fig. 3. 10: Unit Cell under optimization (a) Top view (b) 3-D view

The length of the metal is the first variable under consideration in the study. For this purpose, the length of the metal is first varied from 5 mm to 15 mm while the thickness of the substrate is kept constant at 0.13 mm. This is the minimum thickness of the substrate that can be used for Duroid 5880 and thus the rationale for this value. The unit cell is simulated using Ansys HFSS, and the

simulated S-parameter results are used to extract the dielectric constant values with the help of MATLAB. The results thus obtained are shown in Fig. 3.11.

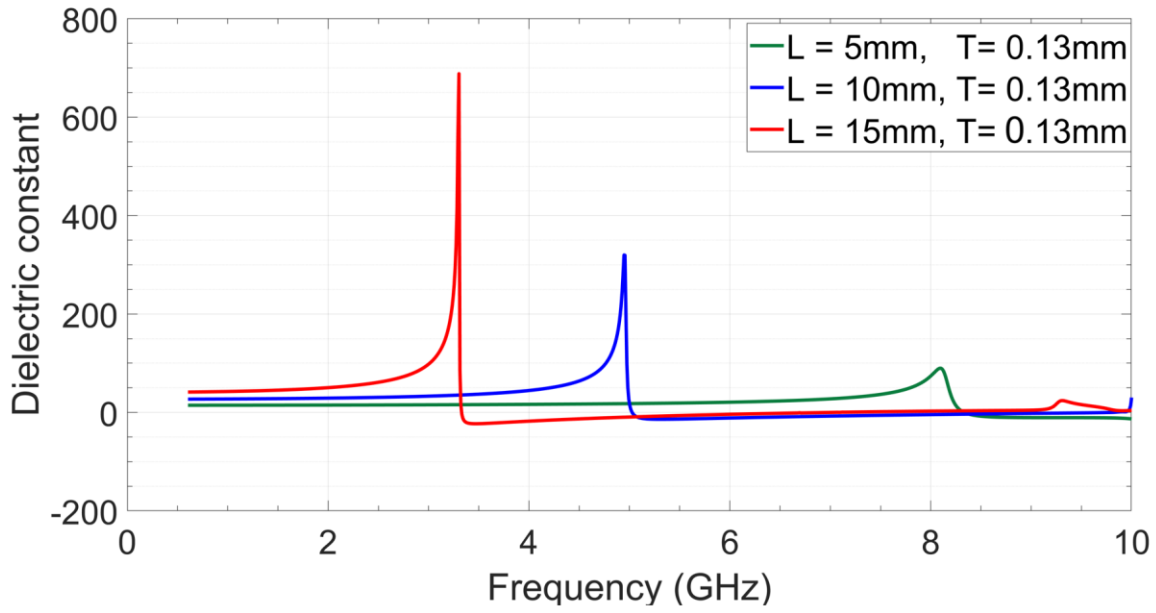

Fig. 3. 11: Simulated effective dielectric constant for change in L (5mm-15mm) while keeping the value of T at 0.13mm

The results shown in Fig. 3.11 are interesting and at the same time quite expected. These simulations show that increasing the length of the metal increases the dielectric constant value but decreases the resonant frequency. The increase in the length of the lines increases the inductance of the unit cell due to which the resonant frequency is seen to be reduced with the increasing length. These results are important to keep an upper limit on the length of the lines. Here, the targeted frequency is 2 GHz, which means that one should use a length value that keeps the resonant frequency well above the targeted center frequency. From this inference, $L = 5$ mm is a good value for the length of the lines. However, this must be re-evaluated once the thickness of the substrate

is studied. It is anticipated that the increasing thickness of the substrate would further lower the resonant frequency. This further rationalizes the length to be kept at 5 mm.

After considering the effect of changing the length of the lines, it is now logical to consider the effective change in the dielectric constant value of the substrate due to the change in the thickness of the substrate. For this purpose, the thickness *(T)* of the substrate was varied from 0.13 mm to 1.57 mm, while the value of *L* is kept constant at 5 mm. The dielectric constant values obtained from these simulations are shown in Fig. 3.12. The values shown in the figure for the thickness are the ones provided by the manufacturer. Therefore, for practical reasons the simulations are carried out using these values.

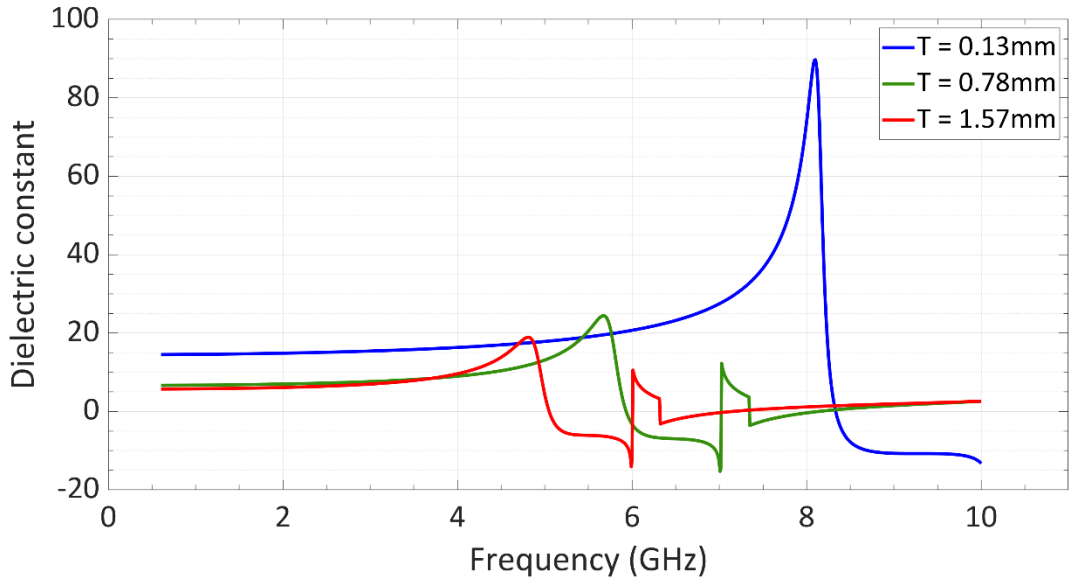

Fig. 3. 12: Simulated effective dielectric constant for change in *T* (0.13mm-1.57mm) while keeping *L* at 5mm

The simulated results shown in Fig. 3.11 illustrate that as thickness increases, the dielectric constant decreases. Similarly, the resonant frequency is also seen to be decreasing with the increasing substrate thickness. For instance, at 2 GHz, it is observed that the dielectric value for L = 5 mm and T = 0.13 mm is 15 (Fig. 3.10), and as the substrate thickness increases to 1.57 mm, the dielectric constant value decreases to 6. For better visualization of the change in the dielectric constant, Fig. 3.13 shows a magnified view of the simulated results. The change in the substrate dielectric constant value is quite encouraging. The greater the percentage change in the dielectric constant value, the more control the RF designer will have on the propagation of the wave.

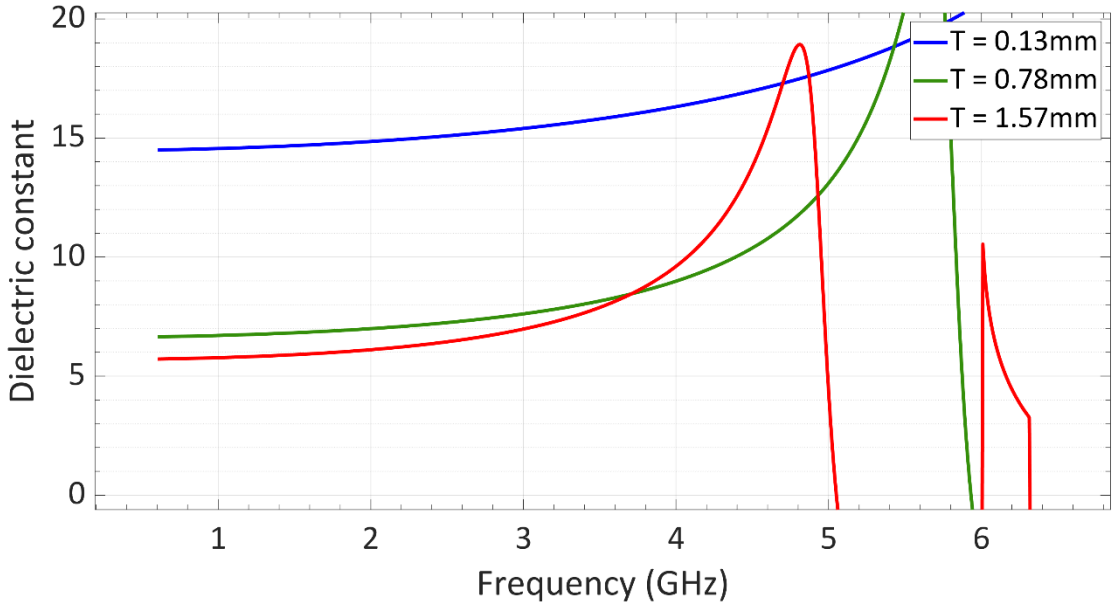

Fig. 3. 13: Magnified view of Fig. 3.12

One final simulation is carried out using dimensions of 3 mm with varying substrate thicknesses. The rationale for this simulation is to observe how compact the unit cell can be designed in this case. For the antenna structure, the plan is to integrate a large number of these unit cell structures.

Therefore, the smaller the size of these cells, the easier it is to integrate them with an RF component. Keeping this in view, the unit cell design of 3 mm is simulated with the maximum thickness of 1.57 mm. The results are added here in Fig. 3. 14. The simulated results presented in this section illustrate the effect of line length and substrate thickness. With these in mind, it is now logical to start varying the capacitor values and then study the extracted properties of the substrate.

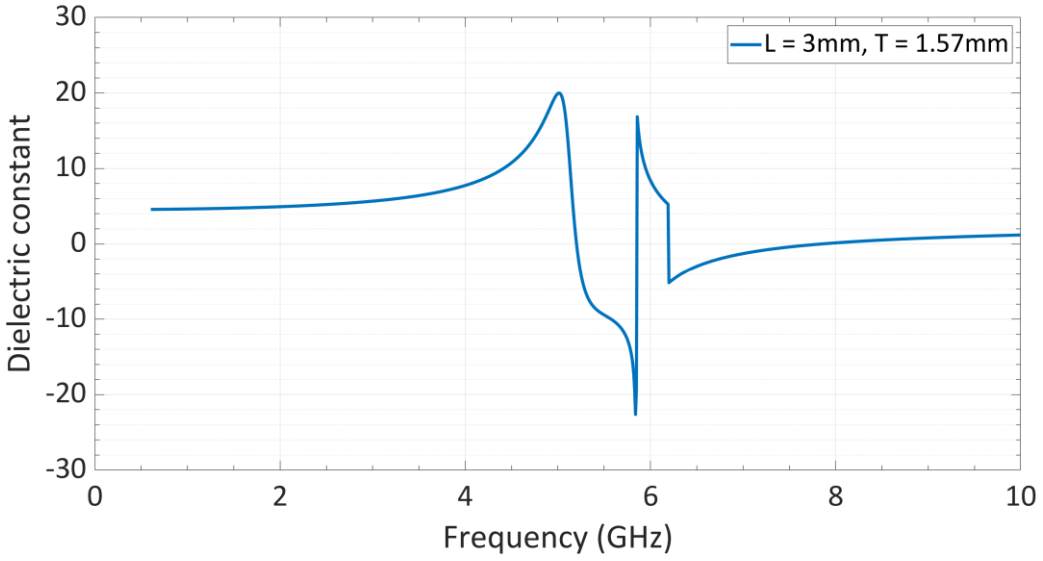

Fig. 3. 14: Simulated dielectric constant of unit cell with L = 3mm and T = 1.57mm

3.2.3 Unit Cell Optimization with respect to Capacitance (C)

After studying the unit cell in terms of L and T, a capacitor is added into the structure at the point of intersection of the two lines, shown in Fig. 3.15. A varactor diode (SMV 1232) from Skyworks Inc. is used for this purpose. The same varactor diode is planned to be used in the actual fabrication. The capacitor is added between the metal conductor line and the ground plane with the help of a via. The via here signifies an RF ground, which will be the anticipated termination on the other

side of the varactor element. While paying attention to the resonant frequency of the unit cell, the capacitance of the integrated varactor (modelled as a capacitor alone) is increased until the resonant frequency is reached. The maximum limit on the resonant frequency is kept at around 2.5 GHz, while analyzing the simulation results. For this purpose, the value of *L* and *T* are kept constant at 3 mm and 1.57 mm respectively, and the change in dielectric constant is studied as shown in Fig. 3.15.

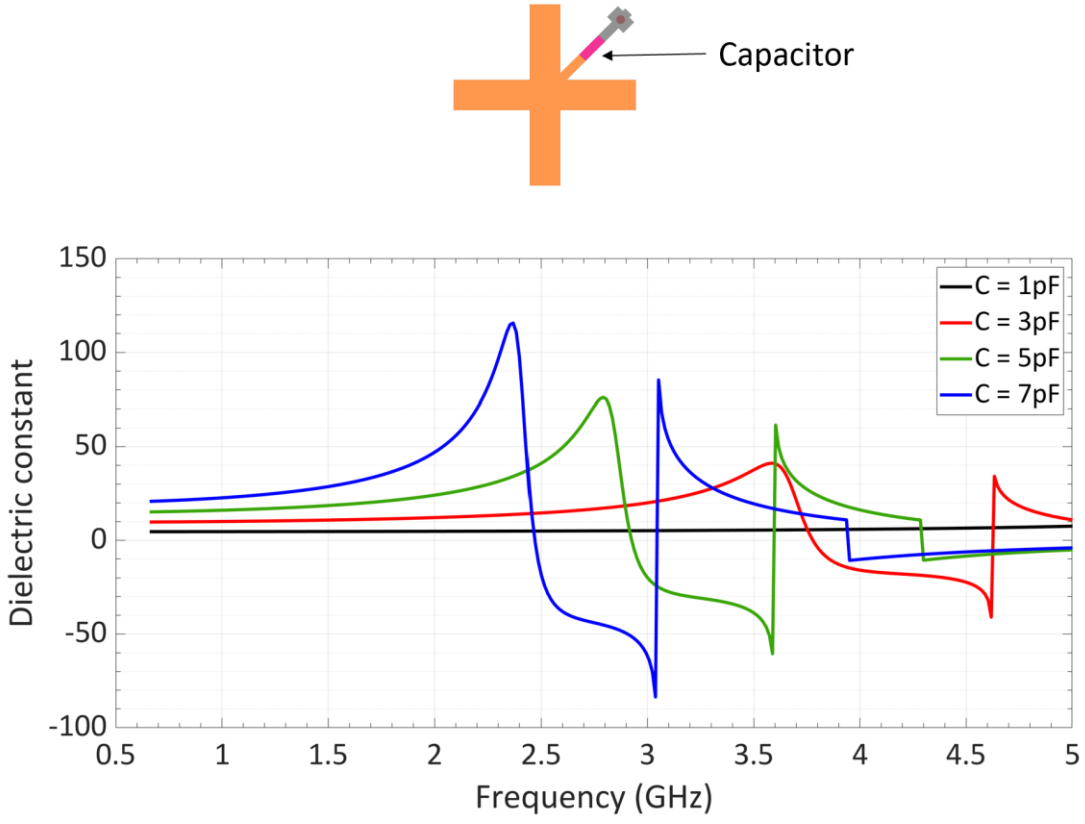

Fig. 3. 15: Change in dielectric and resonance frequency with change in capacitance

It is observed from Fig. 3.15 that with a capacitance value of 7 pF, the resonant frequency is close to 2.5 GHz. Furthermore, at the reference frequency of 2 GHz, the dielectric value is around 50 for 7 pF and increases as the capacitor value increases. So, to be on the safe side and with a good dielectric constant range, a maximum capacitance value of 7pF has been selected. Going beyond 7 pF brings the resonance frequency of the unit cell in the neighborhood of the frequency of interest i.e., 2 GHz. This is not desirable and thus the reason for the upper limit on the capacitance value.

Although a varactor device is usually deemed to be a pure capacitor, in reality that is not the case. Any practical varactor has associated series inductance and resistance values to it. The resistor element is used to model the loss of the varactor which we can ignore in these simulations because generally RF varactors have very low insertion loss associated with them. However, one cannot ignore the series inductance which are modeled in the varactor component. Same is the case with SMV1232 also. The datasheet of the device shows that a 0.5 nH inductance can be used to model the effect of the series inductor introduced by the integrated varactors. Therefore, the next step is to model the effect of the parasitic inductance due to the integrated varactor elements in the unit cell designs.

3.2.4 Unit Cell Optimization with respect to Inductance (L′)

The last step in the study of the unit cell design and optimization is to add an inductive element in series with the capacitor block. This is modeled in Ansys HFSS using an inductor boundary and is shown in Fig. 3.16. The value assigned to this lumped boundary is 0.5 nH as per the datasheet of the SMV1232. Generally, the value of parasitic inductance does not change with the bias voltage and same is the case here with the varactor diode from Skyworks. The unit cell design is re-simulated with the L = 3 mm and T = 1.57 mm with an integrated LC boundary. The capacitance

value is varied again while keeping the inductance constant at 0.5 nH. The extracted substrate parameters are plotted in Fig. 3.16.

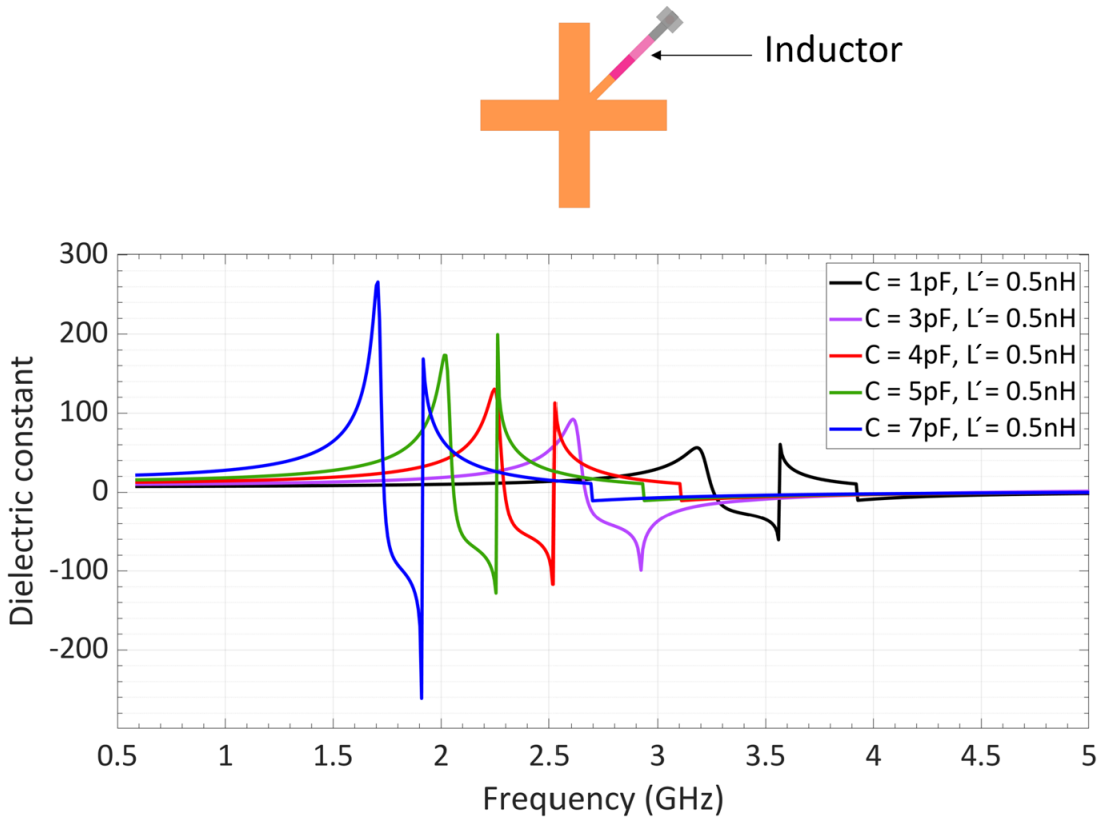

Fig. 3. 16: Change in dielectric and resonance frequency with introduction of Inductor (*L´*)

It can be observed from the Fig. 3.16 that after the introduction of an inductor into the unit cell, the resonance frequency has turned down. For example, in the case of 7pF, without any inductor the resonant frequency was at 2.5 GHz (Fig.3.15), however after the introduction of the inductor, the resonant frequency is shifted to about 1.6 GHz for the same capacitance value. As a result, the highest capacitance value that can now be used is around 3.5 pF while maintaining a resonant frequency of around 2.5 GHz. This is the reason why it is important to model the inductive

properties of the varactor. Before these simulations, it was anticipated that the addition of an inductor can significantly alter the resonant frequency. This has been clearly verified with the help of the last set of simulations.

3.3 Optimized Unit Cell

The final optimized unit cell is shown in Fig. 3.17 that has a capacitor and an inductor attached to it in the form of varactor. The optimized unit cell has a length of metallization to be 3mm, substrate thickness of 1.57 mm and a via of radius 0.07 mm. In the next chapter we are planning to further increase the antenna thickness if required, but for now it is studied for a substrate thickness of 1.57 mm.

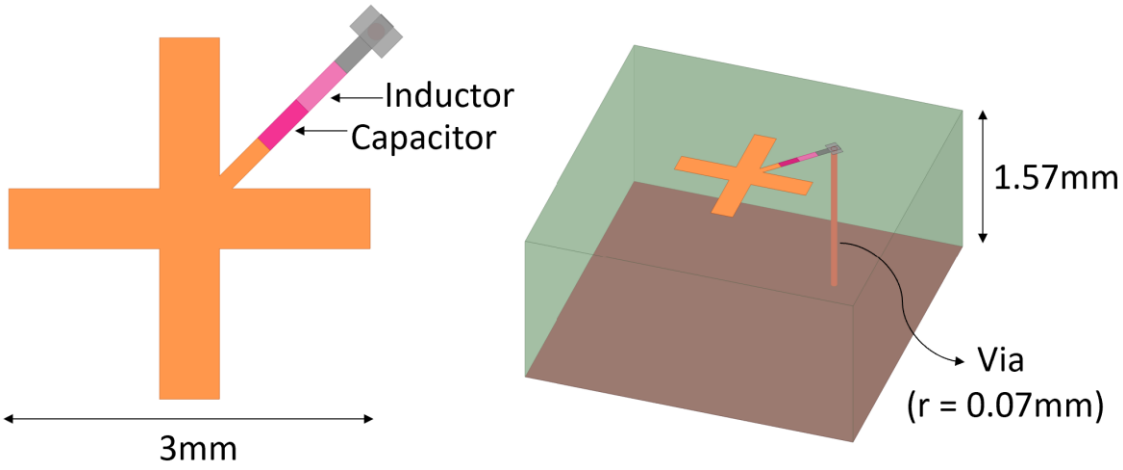

Fig. 3. 17: Optimized Unit Cell

Looking at the effective simulated dielectric constant in Fig. 3.18, the maximum capacitance value that can be used is 4 pF with a resonance frequency of around 2.2 GHz. Looking closely at the dielectric constant values, the dielectric constant of the unit cell is around 20 when the capacitance value is 4pF and decreasing the capacitance value also results in a decrease of the dielectric

constant. Thus, achieving reconfigurability of the unit cell by changing the capacitance value. It should be emphasized here that the substrate thickness used in the unit cell design is 1.57 mm. If the antenna design cannot be optimized for this thickness value, then one needs to revisit the unit cell design with the updated substrate thickness. However, the benefit of this detailed study on the unit cell structure is that changing its substrate thickness to coincide with the antenna substrate thickness will be a trivial step and can be easily done alongside antenna simulations.

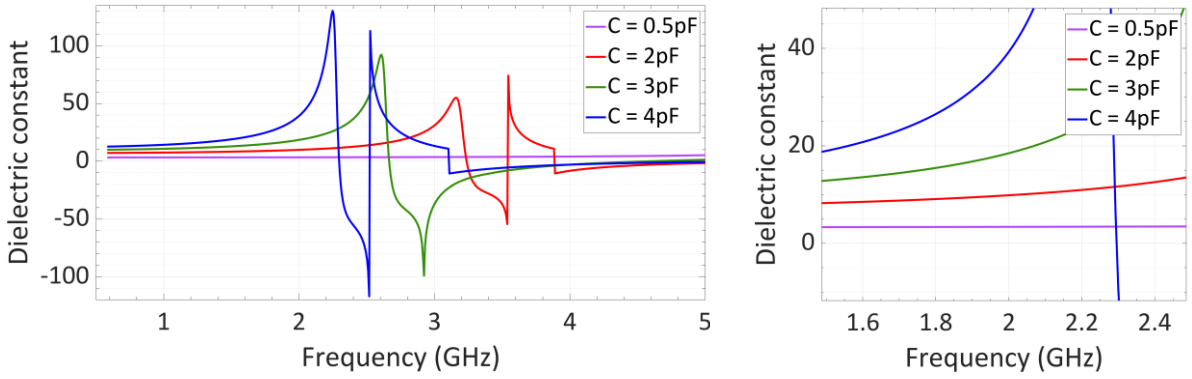

(a) (b)

Fig. 3. 18: (a) Simulated effective dielectric constant of unit cell (b) Magnified view

3.4 Conclusion

A brief overview of FPMS was provided, as well as its unit cell. In FPMS, each unit cell was configured to achieve the reconfigurable waveguide. Unit cell was then optimized to work at the frequency of interest at 2GHz after an in-depth explanation of the unit cell structure and how changing the bias voltages changes the dielectric constant. The optimization process began with a pursuit for the state-of-the art substrate material for substrate, which led to the selection of Duroid 5880. Further optimization includes changes in the length of the metal used while keeping the

width constant, and finally, the introduction of a capacitor and inductor in the form of a varactor to find the maximum capacitance value that can be used while keeping the resonance frequency in mind.

This chapter provides a complete insight into how the unit cell can be designed and optimized for a particular target design. The goal is to use these FPMS unit cells in implementation of an LWA radiator. With the reconfigurability provided by these active elements, it is deemed that a reconfigurable LWA can be realized that can steer its beam at a particular center frequency.

Chapter 4

FPMS based Leaky Wave Antenna Design

LWA's belong to the class of antennas that have the merits of being low-profile, ease of fabrication and an inherent property of frequency beam scanning. However, it is clear from the previous chapters that the focus of this thesis is to steer the beam using an LWA at a single frequency. The primary objective of the research is to propose an FPMS based reconfigurable antenna, therefore it is intuitive to use a structure that relies on microstrip line technology. With the integration of FPMS unit cells onto the antenna structure, a novel LWA design is employed to achieve the radiation pattern reconfigurability in the form of beam steering while keeping the frequency fixed.

At first, an MLWA that has been proposed in [38] is optimized to operate it at the frequency of interest, i.e., 2 GHz. This is followed up by the integration of the FPMS unit cells onto the antenna design. Doing so, it is studied that how the antenna radiation can be controlled by using the active FPMS unit cells. The antenna is studied for its radiation as well as impedance performance and the results thus obtained are illustrated in this chapter.

4.1 MLWA Design

A periodic half-width microstrip leaky wave antenna (MLWA) is demonstrated in [38] and is chosen for study of this thesis. The antenna has the ability of beam scanning to either forward direction or backward direction with the change of frequency. The forward and backward directions in this case are defined along y-axis. This is to say that the main beam can be steered around y-axis. The LWA structure is made up of series of half-width patches (total of 10)

connected by a microstrip line, as shown in Fig. 4.1. The periodic nature of the antenna structure is quite obvious from the diagrammatic illustration. The purpose of this periodicity is to radiate the slow wave out near the edges as it propagates along the structure. The integration of vias at the edge of the line provides the optimum impedance to the propagating wave that results in a particular direction of radiation. The presence of vias in this structure makes it suitable for FPMS unit cell integration and thus the rationale for selection of this antenna. Before the effect of FPMS unit cells is studied on this design, it is advisable to discuss the operating principle of the antenna. This is followed up in the next section.

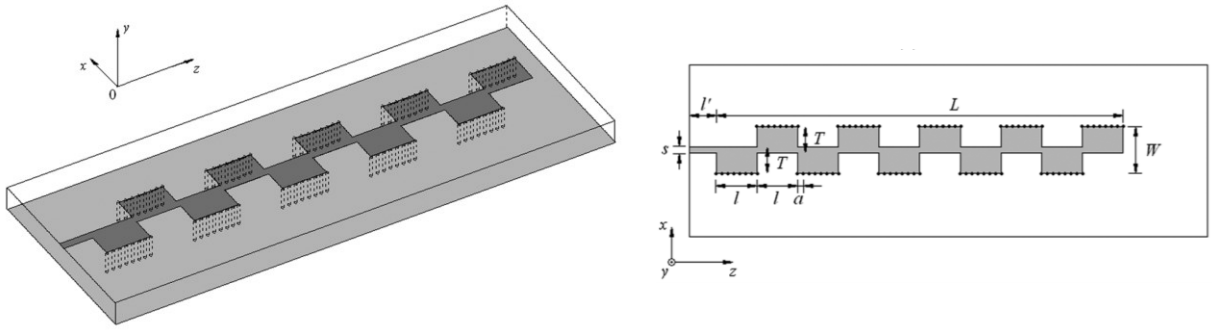

(a) (b)

Fig. 4. 1: (a) 3D view of periodic half-width MLWA (b) The layout of the half-width MLWA [38]

4.2 Theory of MLWA

The periodic loading of the MLWA design is intended to provide the appropriate phase constant (β) of the propagating wave. The structure causes β to vary from negative to positive values as

the operating frequency increases. For a conventional periodic LWA, its complex propagation constant is given by [38]

$$k_{zn} = k_z + \frac{2n\pi}{d}, \quad n = \pm 1, \pm 2, \pm 3 \cdots \tag{4.1}$$

where k_{zn} is given by Eqn. (2.2), k_z is the wave number of the uniform structure, *d* is the period (distance between the repetitive half-width microstrip line) and *n* is the order of the space harmonic.

When compared to a conventional full-width MLWA, the half width MLWA presented has the same radiation characteristic of beam steering with change in frequency, but with the advantage of being smaller in size. However, one would like to study the complex propagation constant of the wave moving on this LWA design. To do so, the first step in calculating the complex propagation constant is to obtain the equivalent extension (*ΔT*) of the half-width MLWA, which varies with operating frequency. In microstrip lines, fringing fields exists at the edge of the structure. These fringing fields depends on the substrate properties such as thickness and dielectric constant *(ε_r)* of the material. By appropriately designing the antenna, the magnitude and phase of the fringing fields can be controlled which in turn results in antenna radiation. *ΔT* of the proposed antenna is given by [38]:

$$\Delta T = 0.412h \frac{\varepsilon_{eff} + 0.3}{\varepsilon_{eff} - 0.258} \frac{\frac{l}{h + 0.262}}{\frac{l}{h + 0.813}} + \Delta \tag{4.2}$$

where *h* is the thickness of the substrate, *a* is the space between each of the vias, *r* is the radius of the vias, *l* is the length of the half-width MLWA, *T* is the width of the half-width MLWA (which

is close to $\lambda_0/4$ for this design), Δ is the expression of the parallel-plate circuit model with a series of vias/shorting pins as given by [38]:

$$\Delta = \frac{a}{2\pi}\left[ln\left(\frac{1}{\pi r}\right) - \frac{4\pi^2 r^2}{a^2} + 0.601\frac{a^2\varepsilon_r}{\lambda_0^2}\right] \tag{4.3}$$

Also, ε_{eff} is the effective dielectric constant that changes with the change in operating frequency and is given by:

$$\varepsilon_{eff} = \frac{\varepsilon_r + 1}{2} + \frac{\varepsilon_r - 1}{2}\left(1 + \frac{5h}{T}\right)^{-(1/2)} \tag{4.4}$$

The complex propagation constant of a wave moving on this MLWA structure has been reported in literature by A. Bhattacharyya and C. Luxey [39], [40]:

$$y_\omega = \frac{h}{120\lambda_0} + j\frac{k_0\varepsilon_r\Delta T}{120\pi} \tag{4.5}$$

$$\exp(jk_x 2T) = -\frac{k_x - \omega\mu y_w}{k_x + \omega\mu y_w} \tag{4.6}$$

Once the value of k_x is calculated with the help of Eqn. (4.6), the complex propagation constant of the uniform half-width MLWA, can be calculated by

$$k_z = \sqrt{\omega^2\mu\varepsilon_r - k_x^2} \tag{4.7}$$

Finally, the angle θ of the main lobe of radiation from the antenna can be calculated by

$$\theta = \frac{\pi}{2} - sin^{-1}\left(Re\left[\frac{\sqrt{\omega^2\mu\varepsilon_r - k_x^2}}{k_0} - \frac{\lambda_0}{d}\right]\right) \tag{4.8}$$

The analysis presented above basically entails that as the frequency of the wave propagating through the antenna is varied, the complex propagation constant (k_z) inside the substrate will

change. The change in k_z is due to the varying k_x value. Thus, as the frequency of the input signal modifies, the direction of the main beam given by Eq. (4.8) will change and this direction can be controlled by appropriately designing the structure to provide the right value of k_x.

For this work, instead of changing the frequency of the input wave, the idea is to modulate the substrate properties (ε_{eff}) using the FPMS unit cells in Eq. (4.2). As a result, the value of fringing fields 'ΔT' can be controlled. As the value of 'ΔT' varies, the complex propagation constant of Eq. (4.5) and (4.6) will change. The conclusion can be drawn from Eq. (4.8) where the direction of radiation *'θ'* depends on the propagation constant or in other words on 'k_x'. As k_x changes so does the angle of antenna radiation. It is noteworthy to mention it here that the analysis here is being done considering that frequency of the antenna and the wavelength (λ_0) are constant. One limitation of this model is that it can only be applied to a homogenous material with a uniform dielectric constant. This is different from the study that this thesis aspires to pursue. However, once the simulated results are presented a comparison between the theoretical model and the simulated results will be presented to validate the simulation model using the theory proposed in [38].

4.3 MLWA Optimization

The theoretical understanding of the MLWA of Fig. 4.1 is important to understand the antenna behavior. Therefore, this can be followed up by the optimization of the antenna design, first without FPMS unit cells to the frequency of interest. The optimization process begins with a reproduction of the reference antenna design [38] into the full wave solver Ansys HFSS and a comparative analysis. At first, the dimensions of the antenna that are reported in [38] are used to model the structure in the simulator. By carefully defining the right simulation environment the

antenna is simulated to understand its radiation properties. For the most part, it is concluded that the antenna works well between 4.5 to 5 GHz for backward radiation and from 6.5 GHz to 8 GHz for forward radiation. This is in close agreement with the measured results of the reference article. In addition, it validates the simulation model that has been reproduced using HFSS and provides a certain degree of confidence that any results obtained here onwards are generally reliable. Once the design results have been largely reproduced, the actual designing process of this work starts with optimizing the antenna to operate at the target frequency of 2GHz.

The antenna's impedance and radiation characteristics depend mainly on its parameters in terms of *L, l, T, l', a, s* and *W* (shown in Fig. 4.2(a)). Duroid 5880 is used for the design process with a substrate thickness of 0.8mm. Initially, this substrate thickness is selected to not deviate much from the original design. The other dimensional modifications are made in such a way that the antenna radiates at 2 GHz. For example, the value of *'T'* is dependent on the wavelength of the signal. By basic calculations, the right value for this dimension is chosen. Similarly other variables are modified to achieve the desired results of radiation. A brief summary of these dimensions are shown in Fig. 4.2(a). In terms of radiation pattern, the simulated results show a very good gain of about 13.5 dBi as shown in Fig. 4.2(c). These results are encouraging as the antenna performance is properly established through them. Having written that, despite having a high gain, the antenna is not properly matched in terms of its impedance, as shown in Fig. 4.2(b). At 2 GHz, the reflection coefficient of the simulated antenna is about -2.5 dB, which is well above the acceptable IEEE norm of at least -10 dB. This needs to be corrected before the integration of FPMS unit cells on the antenna design. Also, the current size of the antenna shows a length of 660 mm. This is too long for practical handling of the antenna and its characterization. Therefore, this also needs to be improved while keeping in view the real-world constraints in mind.

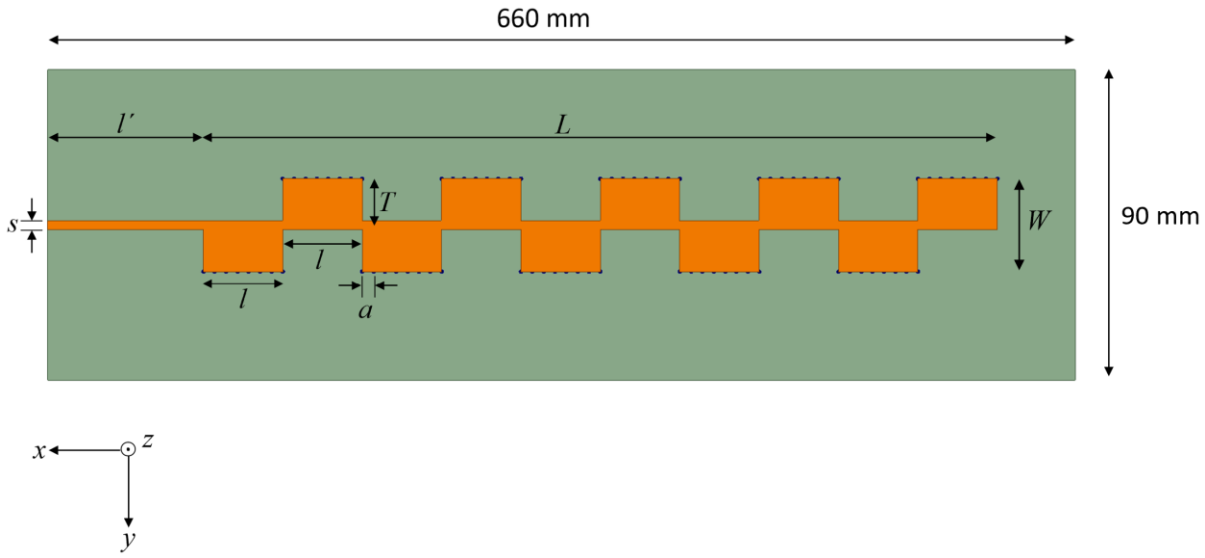

(a)

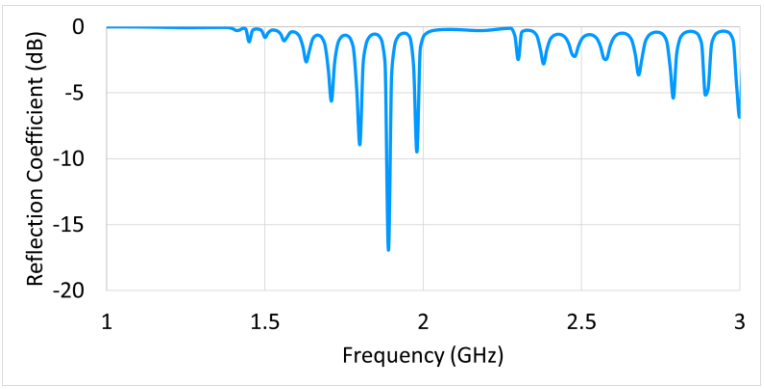

(b)

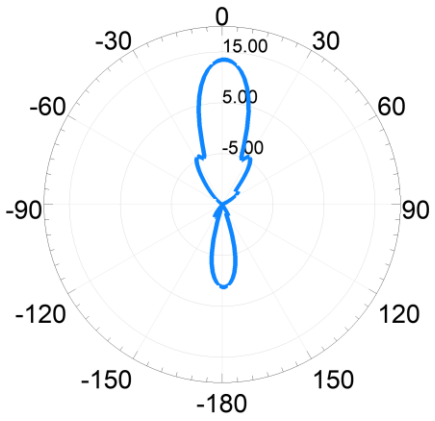

(c)

Fig. 4. 2: (a) Optimizing antenna (L = 510mm, l = 51 mm, T = 30 mm, l' = 100 mm, a = 7.3 mm, s = 6 mm and W = 60 mm (b) Simulated reflection coefficient (c) Simulated radiation pattern with a gain of 13.5 dBi

The next step is to reduce the antenna size (length) and optimize the reflection coefficient to at least -10 dB. Various methods for reducing the size of the antenna are investigated. At first the number of patches used in the antenna is reduced from 10 to 3. This can greatly reduce the overall length of the antenna. A close eye is kept on the antenna radiation pattern and the reflection

coefficient. Following comprehensive customization, for 3 patches having a total length of 335 mm and a width of 120 mm, with substrate thickness of 1.5 mm, and with an increased via radius of 4 mm is deemed to be a good design (shown in Fig. 4.3(a)).

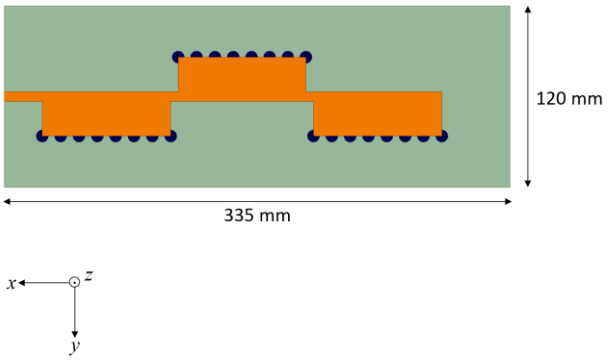

(a)

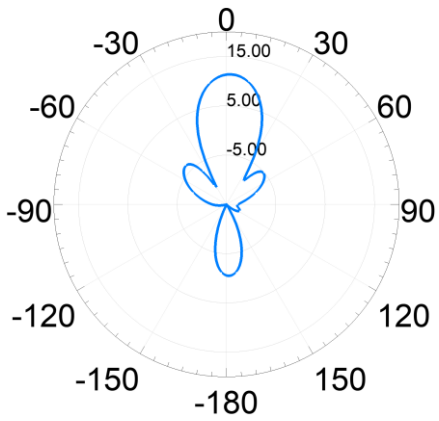

(b)

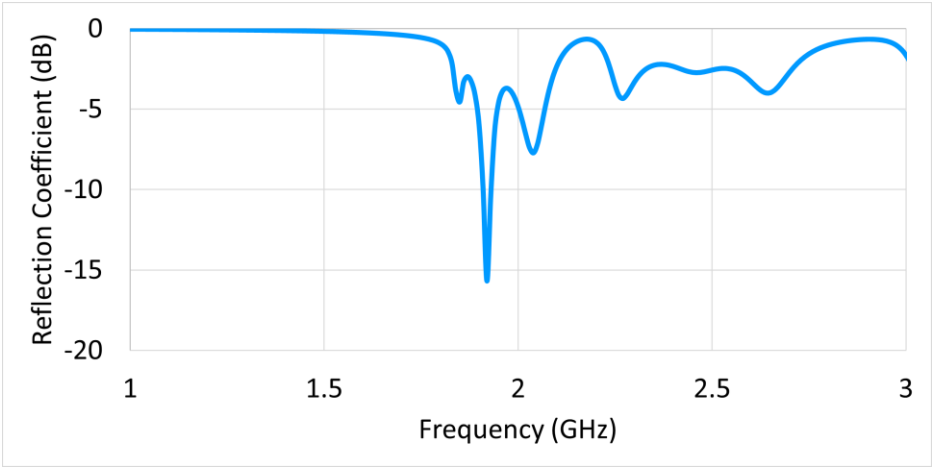

(c)

Fig. 4. 3: (a) Optimizing antenna with 3 patches with L = 265 mm, l = 85mm, T = 26 mm, l' = 25 mm, a = 12 mm, s = 6 mm and W = 52 mm (b) Radiation pattern with a gain of 11.3 dBi for 2GHz (c) Simulated reflection coefficient

These optimization steps do allow the antenna size to come within acceptable range. However, despite the fact that the antenna's size has been reduced to a significant value and it has a strong radiation gain of about 11.3 dBi, does not mean that the antenna is operating at its best. This is illustrated by the antenna's impedance performance shown in Fig. 4.3(c), where the value is -4 dB at 2 GHz. Thus, as the antenna size is manageable now, the next focus of optimization will be on the antenna's impedance.

As mentioned before that the minimum acceptable target of -10 dB reflection coefficient must be achieved. The antenna design reported in [38] is designed to operate at high frequencies (all the way up to 8 GHz) and therefore the substrate thickness employed there is 0.8 mm. For this work, the designed frequency is much lower (2 GHz) and therefore to induce proper radiation from the antenna, it is possible that a thicker substrate can be used. Keeping this in view, the substrate's thickness is now given the attention. The antenna thickness is varied with the implementation of the Duroid 5880 to investigate its effect on the reflection coefficient. As the thickness of the antenna is increased from 1.5 mm to 3.96 mm, the impedance matching improves with a reflection coefficient of about -15 dB as shown in Fig. 4.4(c). The value of 3.96 mm is used while keeping an eye on the actual substrate thicknesses available from the manufacturer. Duroid provides 5880 substrates with thicknesses of 3.175 mm and 0.787 mm. When combined together, these two values will result in a thickness of 3.962 mm. Also, while optimizing the antenna impedance, it is important to take care of the antenna's radiation characteristics. Throughout these simulations, it is seen that the antenna radiation is not affected much by the substrate thickness variations. With the improved matching, the antenna provides a stable gain of 11 dBi with the same beamwidth as is shown in Fig. 4.6(b).

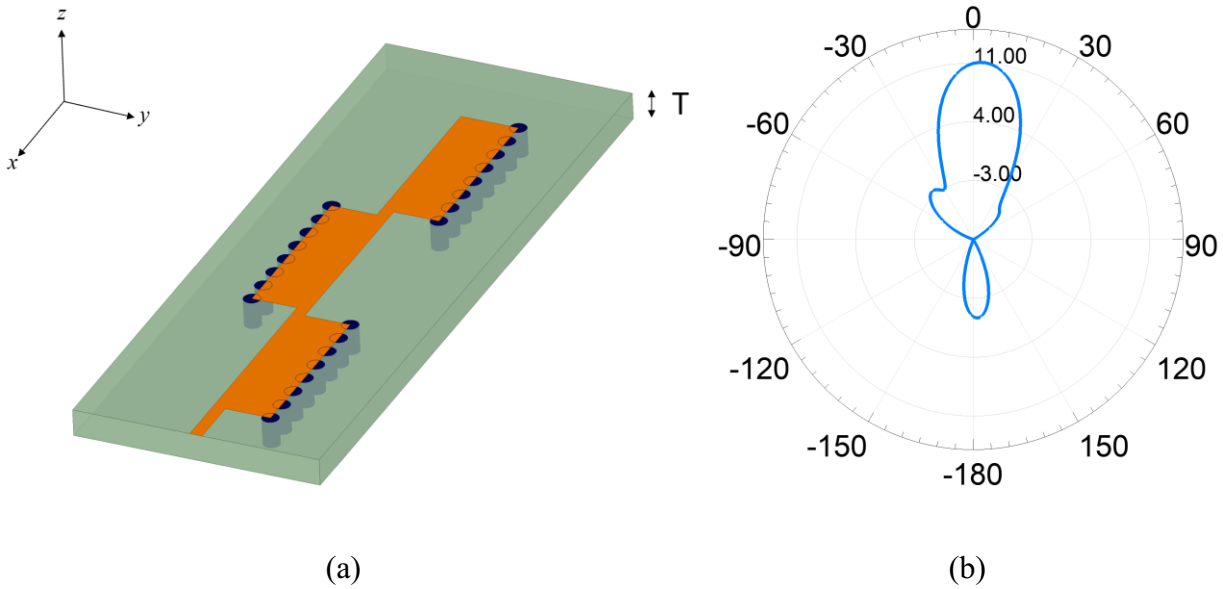

(a) (b)

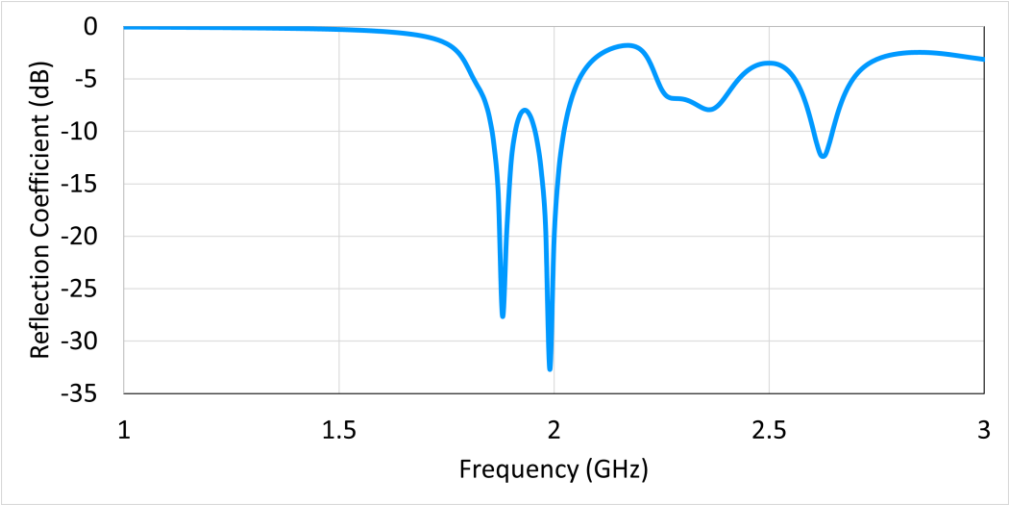

(b)

Fig. 4. 4: (a) Simulated antenna with thickness *T*. (b) simulated radiation pattern with gain of 11 dBi (c) Simulated reflection coefficient of antenna with substrate thickness of 3.96mm

In this way the reference antenna is optimized to be working at 2 GHz with its miniaturized version, acceptable reflection coefficient and high radiation gain. With this the next logical step is to

incorporate the FPMS unit cell into this antenna design to achieve beam steering with a fixed frequency.

4.4 Integrating FPMS Unit Cell into Antenna

FPMS unit cells are integrated onto the MLWA structure in place of the vias at the edge of the structure. This is done in a sequential manner by replacing the vias with the unit cells of one patch at a time. Addition of too many variables in a single attempt is not advisable as it makes it hard to decipher the effect of each variable on the antenna results. Therefore, this strategy of replacing one stream of the vias at a time is used to gradually study the change in the antenna radiation pattern.

The FPMS unit cell is re-simulated using the new 3.96mm substrate height, and the simulated dielectric constant is shown in Fig. 4.5. The resonance frequency has shifted to around 2.4 GHz for 3pF due to the increased substrate height. As a result, while studying the antenna, the capacitance of the varactor at maximum can be increased to around 3.5 pF or close to it.

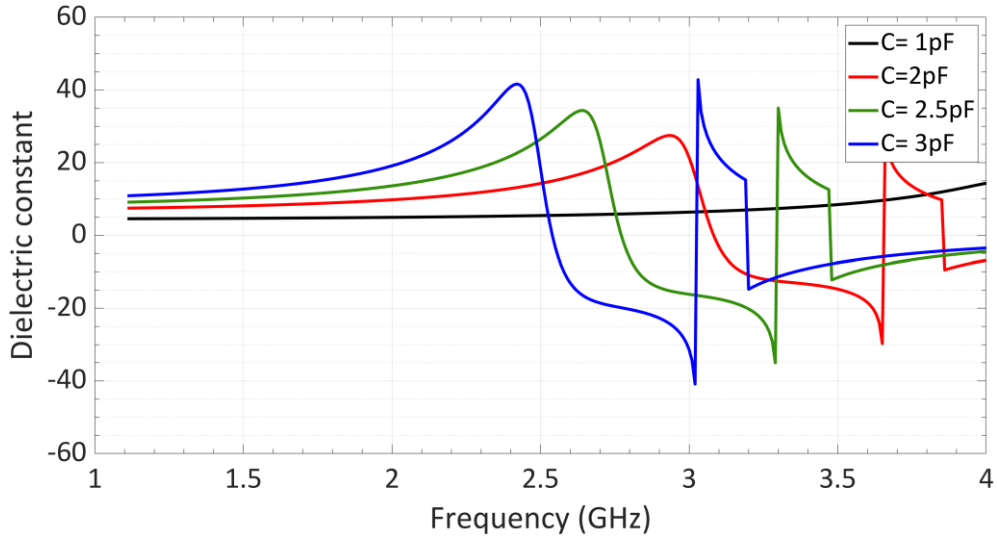

Fig. 4. 5: Simulated dielectric constant of FPMS unit cell with substrate thickness of 3.96mm

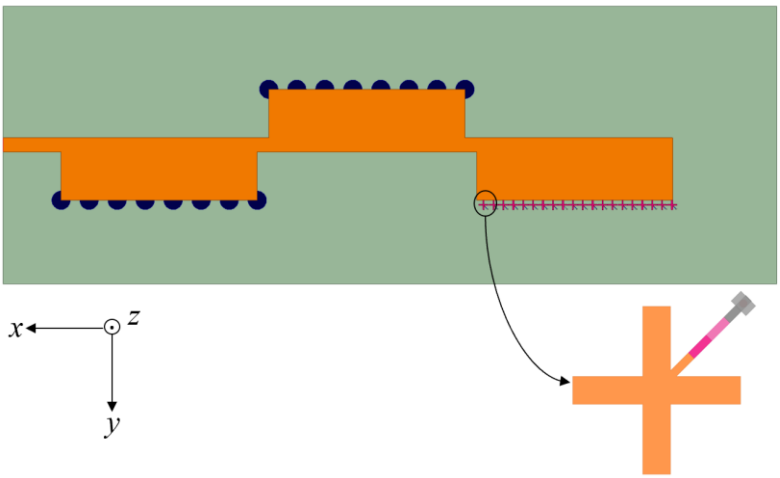

(a)

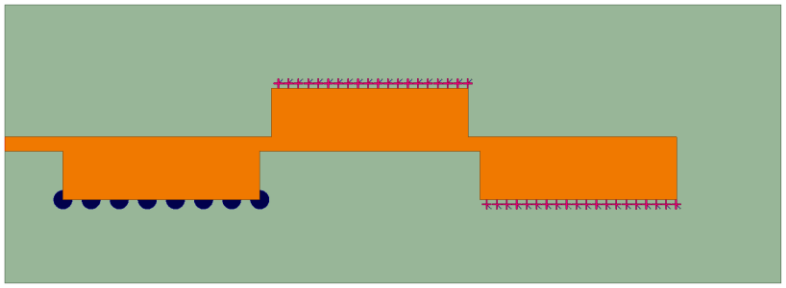

(b)

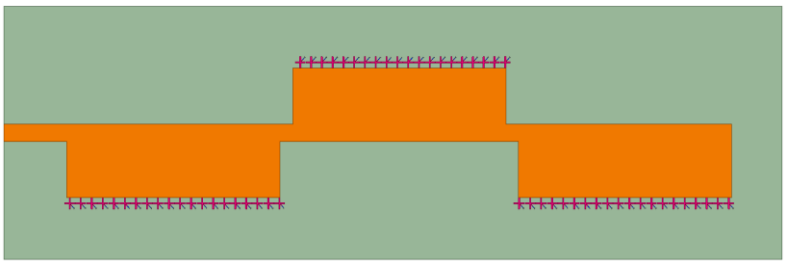

(c)

Fig. 4. 6: (a) Antenna with 20 FPMS unit cells on one patch (b) Antenna with 20 FPMS unit cells on two patches (c) Antenna with 20 FPMS unit cells on all three patches

A few trial variations are shown in Fig. 4.6, where the FPMS unit cells are integrated in one patch (Fig. 4.6(a), two patches (Fig. 4.6(b), and three patches respectively (Fig. 4.6(c). A total of 20 FPMS unit cells have been implemented in each of the three cases as shown in Fig. 4.6. The simulated results of the beam steering and reflection coefficient are studied for all the three antenna designs. The reason for using 20-unit cells is due to the size limitation of the patches. This is the maximum no. of unit cells that can added onto the antenna structure. Also, it is important to mention that, more the no. of unit cells, the better control can be achieved on the antenna characteristics. Therefore, maximum no. of cells that can be crowded onto the patch are used for simulation purposes. While looking at the results, it is seen that the integrating unit cells on one patch only results in minimum beam steering of the antenna radiation. As the unit cells are integrated onto the second patch, the beam scanning increases to 10° when same capacitance value is used in all the FPMS unit cells. However, the best steering results are obtained from the last design where a total of 32° is observed, shown in Fig.4.7. The capacitance values in all these simulations are varied from 2 pF up to 3.5 pF. The rationale for this choice is quite obvious from Fig. 4.5. All the results reported here show beam steering in backward direction. These results provide the first step towards the proof-of-concept of an FPMS based antenna. However, some more optimization and study are needed to get to the final results.

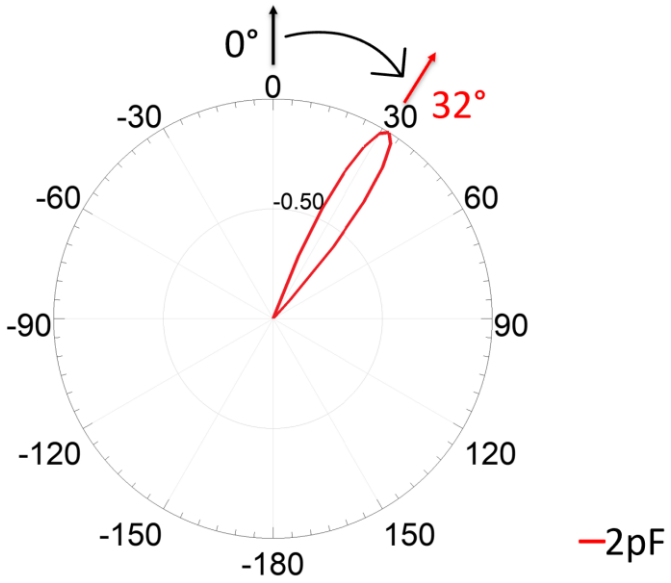

Fig. 4. 7: Simulated radiation pattern of 4.6(c)

Also, as discussed in Chapter 2, the objective of this work is to obtain continuous beam scanning in both the forward and the backward directions, or from left to right and vice versa. Thus, the design also needs to be explored to provide the desired continuous beam steering.

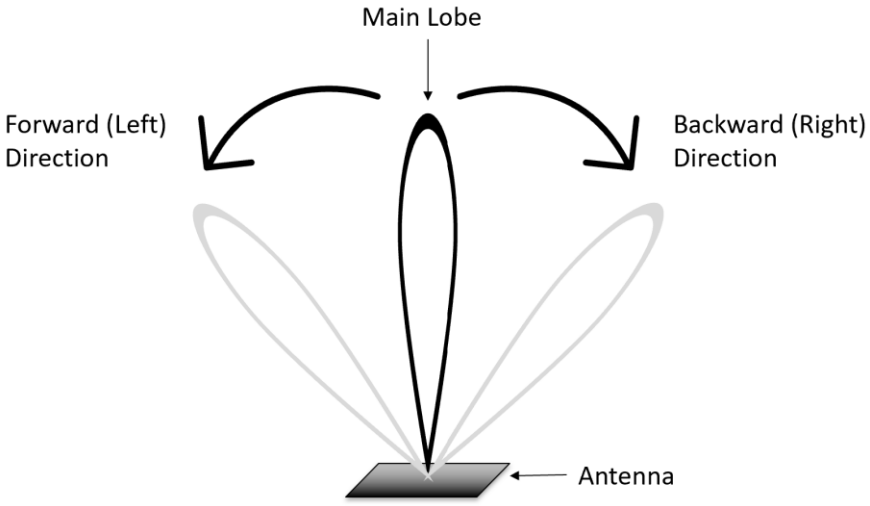

Fig. 4. 8: Beam Steering of main lobe

4.4.1 Radiation Beam Steering in Backward (Right) Direction

The beam steering of the main lobe is achieved after experimenting with different combinations and placements of unit cells along with the via of radius 4 mm. The best beam steering results are obtained for the case when all three patches have FPMS cells integrated on to them. However, in this case the antenna reflection coefficient does not show optimum impedance matching. To improve the antenna matching, the patch near the feed of the antenna is only integrated with unit cells along the half of its length. The remaining half that is right adjacent to the feedline is left unaltered with vias (not using FPMS unit cells). Such a design is expected to show better impedance results since the RF wave does not go through a sudden impedance change when it enters into the antenna structure. This design configuration is shown in Fig. 4.9. The geometry consists of 50-unit cells total, 20 on the upper patch, 20 on the lower rightmost patch, and 10 on the leftmost lower patch. The first half of the first patch consists of a total of 15 vias with 1 mm of radius each. The radius of the via attached to the design was reduced from 4 mm to 1 mm in this design for improved results and ease of fabrication.

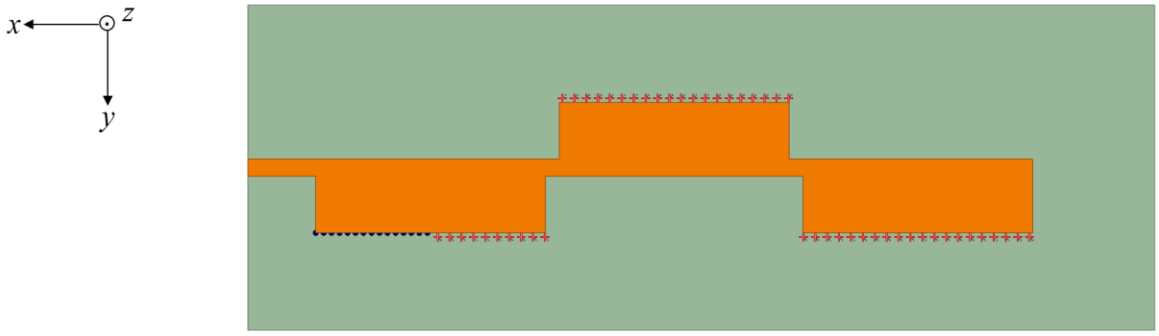

Fig. 4. 9: Antenna design with 50-unit cells and 15 vias of 1mm radius

The normalized radiation pattern results of the antenna (Fig. 4.9) are shown in Fig. 4.10. As the capacitance of the FPMS unit cell is varied, the main lobe of the antenna radiation steers from 0° to 32° (with reference to boresight direction). The capacitance in this case is varied from 2.2 pF to 3.3 pF. These values of the capacitance are such that the antenna produces best radiation results. If different values are used, then not much of steering is observed from the antenna. This means that the variation of the unit cells beyond this range of capacitance does not alter the wave impedance of the RF signal propagating through the antenna structure. Therefore, this range is optimum to attain the best results of beam steering. During this steering, the maximum antenna gain is seen to be 11 dBi with a variation of around 3 dB in the maximum radiation direction. It is also worth noting that the side lobe level of the antenna radiation increases by 6 dB as the beam steering angle of the main beam varied from 0° to 32°. This increase in the side lobe levels is quite expected and causes the reduction in the gain of the main antenna beam. In this case, the antenna is steered until the side lobe level is at least 3 dB less than the main beam. These radiation characteristics are quite acceptable as per IEEE standards.

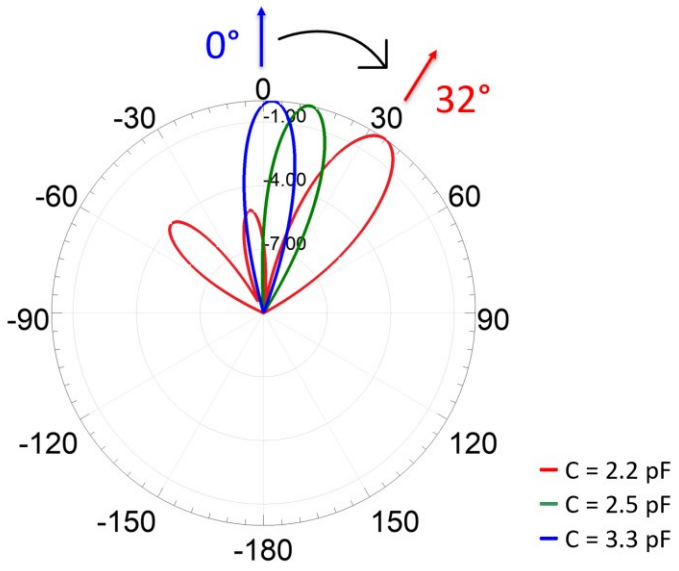

Fig. 4. 10: Normalized Radiation pattern of antenna design with 50-unit cells and 15 vias of 1mm radius.

After discussing the radiation characteristics of the FPMS based MLWA, shown in Fig. 4.10, its quite natural to discuss the simulated reflection coefficient. That explains the impedance performance of the antenna. It is observed that the antenna has suitable impedance matching for capacitance values of 2.5 pF and 3.3 pF, with values of -19 dB and -15 dB, respectively, but not for capacitance value of 2.2 pF at 2 GHz as shown in Fig. 4.11. At 2.2 pF the reflection coefficient demonstrates a value of -7 dB. According to the IEEE standard, the minimum acceptable reflection coefficient value is -10 dB. Therefore, this parameter needs to be corrected for the optimized antenna performance.

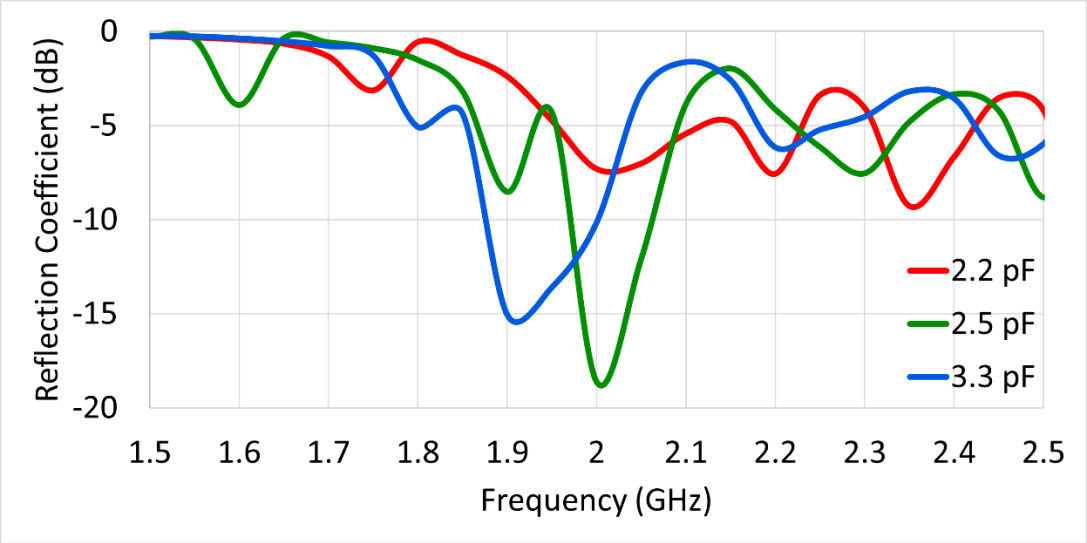

Fig. 4. 11: Reflection coefficient of antenna design with 50-unit cells and 15 vias of 1mm radius

To accomplish the optimized antenna impedance performance, a tapered feeder, as shown in Fig. 4.12, is added to the input of the antenna design. With the help of Ansys HFSS a parametric study is carried out to determine the best feeder dimensions. The optimal feeder dimensions is in the

form of a triangle with 7 mm in base and 18 mm in height. In addition, it is seen that increasing the no. of vias at the input also helps to improve the input reflection coefficient.

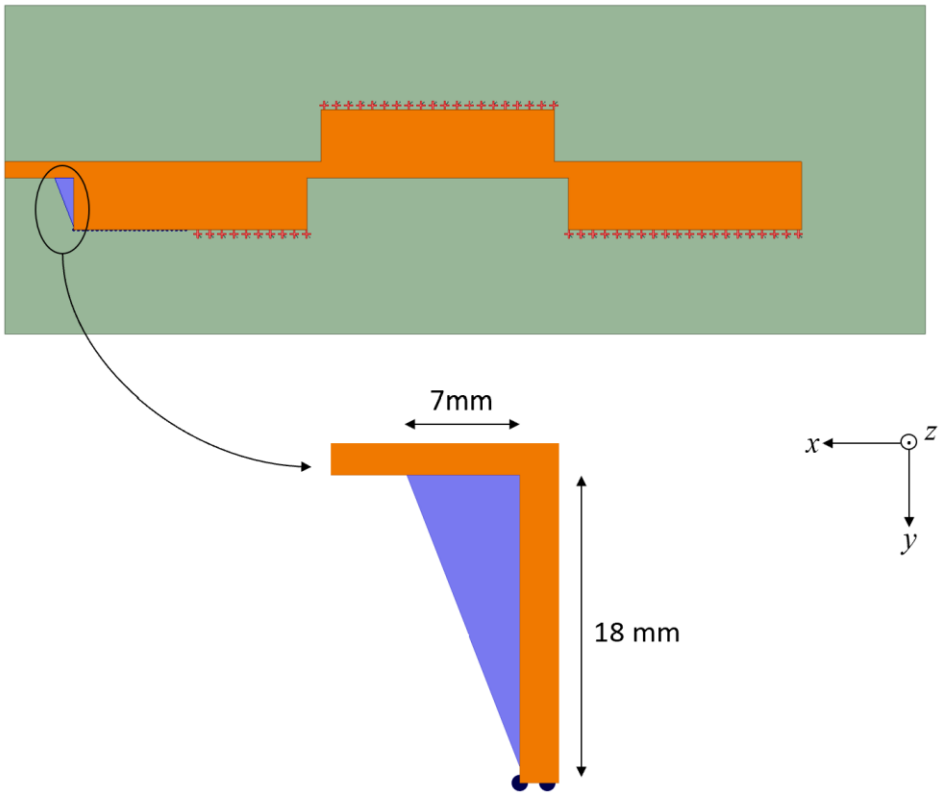

Fig. 4. 12: Antenna design with Feeder

The addition of the feeder significantly improves impedance matching as shown in Fig. 4.13. The reflection coefficient for a capacitance value of 2.2 pF is now -11dB, which is within the IEEE standard range. Further looking at the reflection coefficient values for the capacitance vales of 2.5 pF and 3.3 pF, the values are -14 dB and -10.5 dB, respectively. When one compares these results with the reflection coefficient of the antenna without feeder, it can be deduced that the impedance matching for capacitance values of 2.5 pF and 3.3 pF have degraded somewhat. However, the difference for these two cases is minor when compared to the overall impedance matching for all

three capacitance values. Also, since the IEEE standard is met in all three cases, therefore it is better to use this design as compared to the last one.

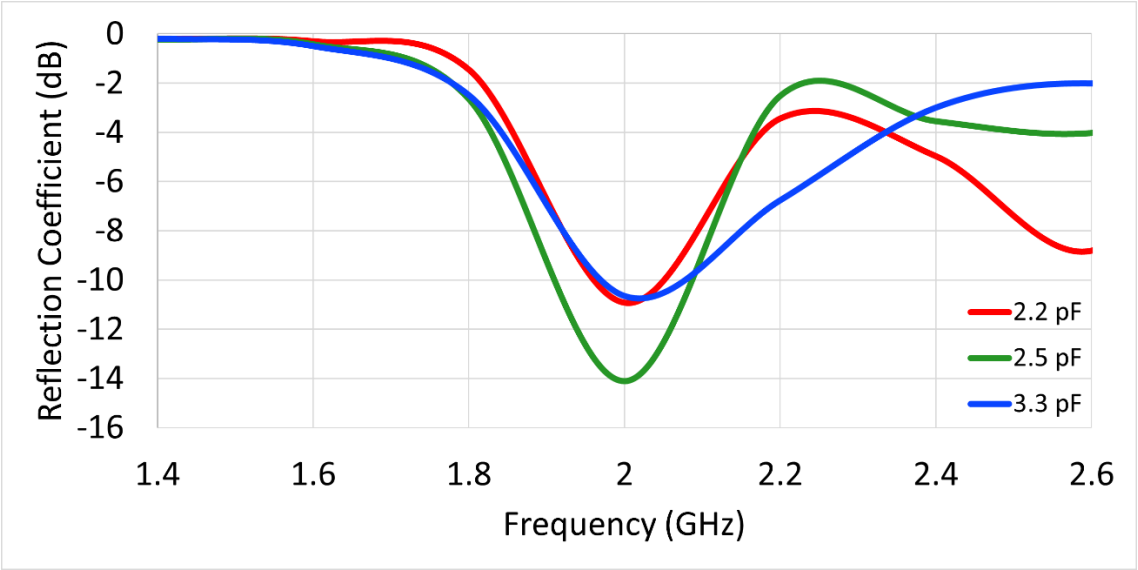

Fig. 4. 13: Reflection Coefficient of antenna design with Feeder

Although the integration of the feeder helps to improve the impedance matching for all values of capacitance of the unit cell, one also has to pay attention to the radiation performance of the antenna. When looking at the effect of the feeder on the radiation pattern, it can be seen that there is not much change in the radiation pattern in terms of the direction of the main beam and the gain of the antenna. For 3.3 pF capacitance value, the antenna radiates in the boresight direction (0°) with a gain of 10.5 dBi. Reducing the capacitance value to 2.5 pF and 2.2 pF results in a steered beam of 15° and 30° with a gain of 10.5 dBi and 8.5 dBi, respectively. Thus, with a gain variation of 2 dB the antenna provides a beam steering of almost 30° with acceptable input matching. For

easy visualization, the normalized radiation pattern is illustrated on Fig. 4.14 with a beam steering of 30°.

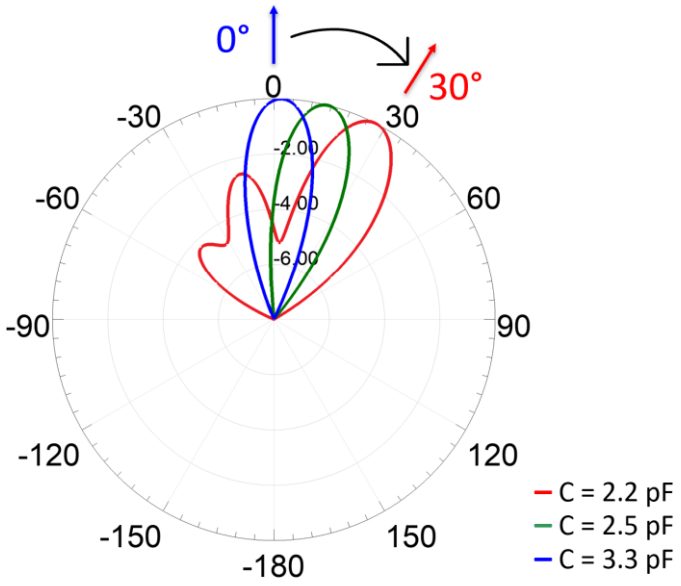

Fig. 4. 14: Simulated normalized radiation pattern with feeder and beam steering on backward (right) direction

4.4.2 Radiation Beam Steering in Forward (Left) Direction

The steering of the main lobe of the antenna in the forward direction needs to be investigated after successfully steering the radiation beam to the backward direction. Different capacitance values of the unit cells are studied to obtain continuous beam steering to the left of the bore-sight. Instead of adjusting the capacitance value of all 50-unit cells together at a time, different sets of capacitance values are allocated, as shown in Fig. 4.15. *C*1 refers to the capacitance values of the 30-unit cells on the right of the antenna axis (lower side), while *C*2 refers to the capacitance values of the 20-unit cells on the left of the antenna axis (upper side). Different possible combinations of

*C*1 and *C*2 are employed in order to find the best possible combination to achieve continuous beam steering on the left side while maintaining good impedance matching.

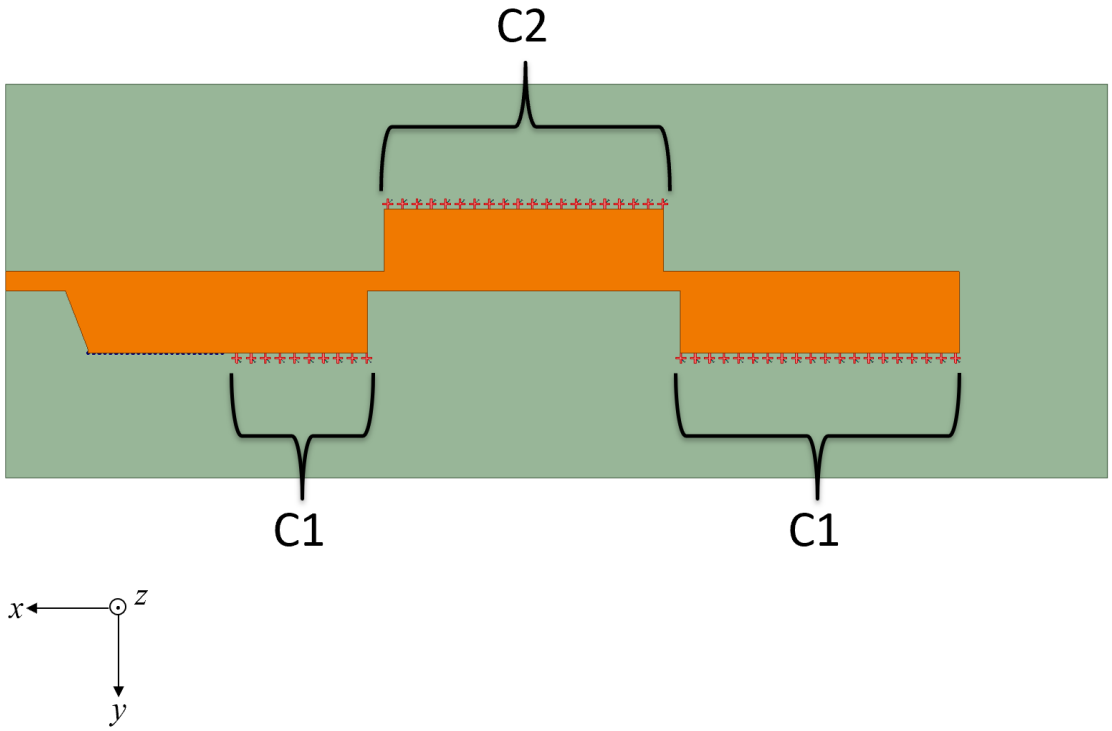

Fig. 4. 15: Different sets of Capacitance value for FPMS unit cells

A continuous beam steering of -30° on the left side is obtained by keeping *C*1 constant at 2.4 pF and varying *C*2 up to 0.6pF. The main radiation beam is steering with an angle of -15° and -30° from the bore-sight with values of *C*2 equal to 0.2 pF and 0.6 pF, respectively, while keeping *C*1 fixed at 2.4 pF, as shown in the Fig. 4.16. The main lobe gain is 9 dBi at -15° and 8 dBi at -30°, with a maximum gain variation of 2.2 dB. Increasing the capacitance value above 0.6 pF results does not provide any further steering. To achieve acceptable antenna gain and radiation performance, these capacitance values are used here. The capacitance values used in this case to demonstrate steering on the left side is determined with the help of series of HFSS simulations.

For this purpose, a parametric study is performed on the values of $C1$ and $C2$. The results shown in Fig. 4.16 are obtained due to this set of simulations.

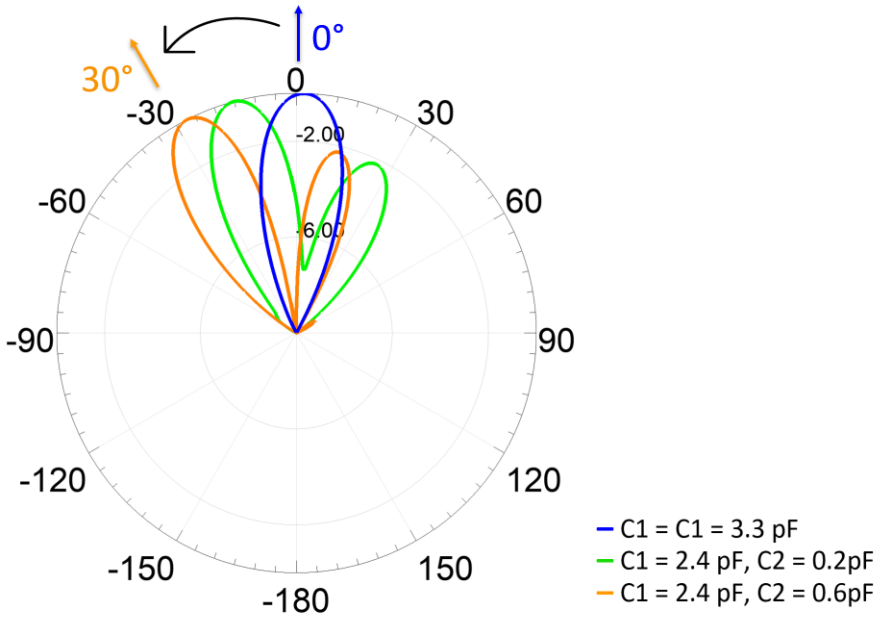

Fig. 4. 16: Simulated normalized radiation pattern on forward (left) direction

Further looking at the reflection coefficient of the radiations at an angle -15° and -30° are -10.5 dB and -11.5 dB, respectively as shown in the Fig. 4.17. These results are again within the IEEE standard of at least -10 dB and exhibit that the antenna is matched under these conditions

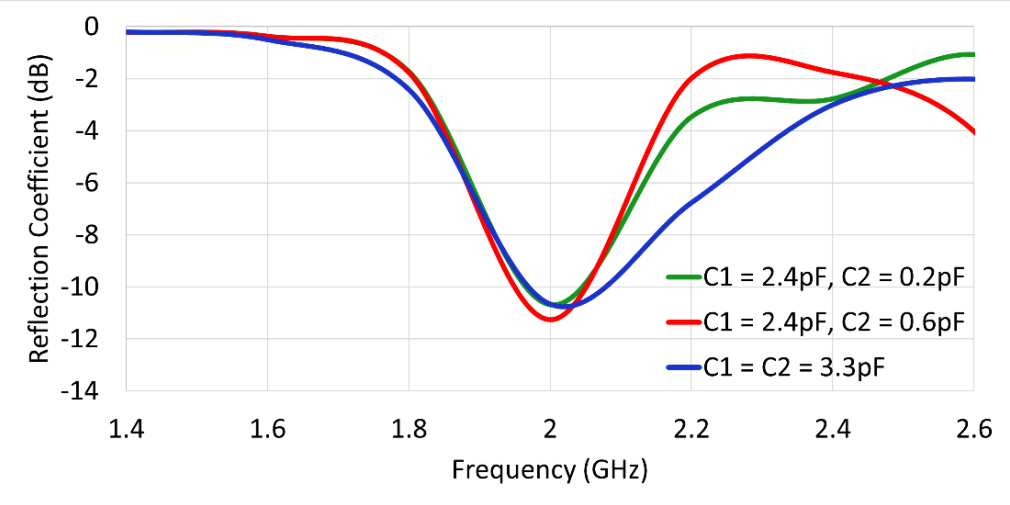

Fig. 4. 17: Reflection coefficient for forward steering of MLWA

4.5 Final Antenna Design

The final optimized antenna design that can steer the main lobe of the radiation in ±30° is shown on the Fig. 4.18 with a length of 335 mm and width of 120 mm. It consists of a total of 50 FPMS unit cells and 25 Vias of 0.5 mm radius in the first patch. Each unit cell has an inductor and capacitor in the form of varactor along with a via of radius 0.07 mm. A feeder is attached into the design for better impedance matching. The substrate material used is Duroid 5880 with a relative permittivity of 2.2 and a dielectric loss tangent of 0.0009.

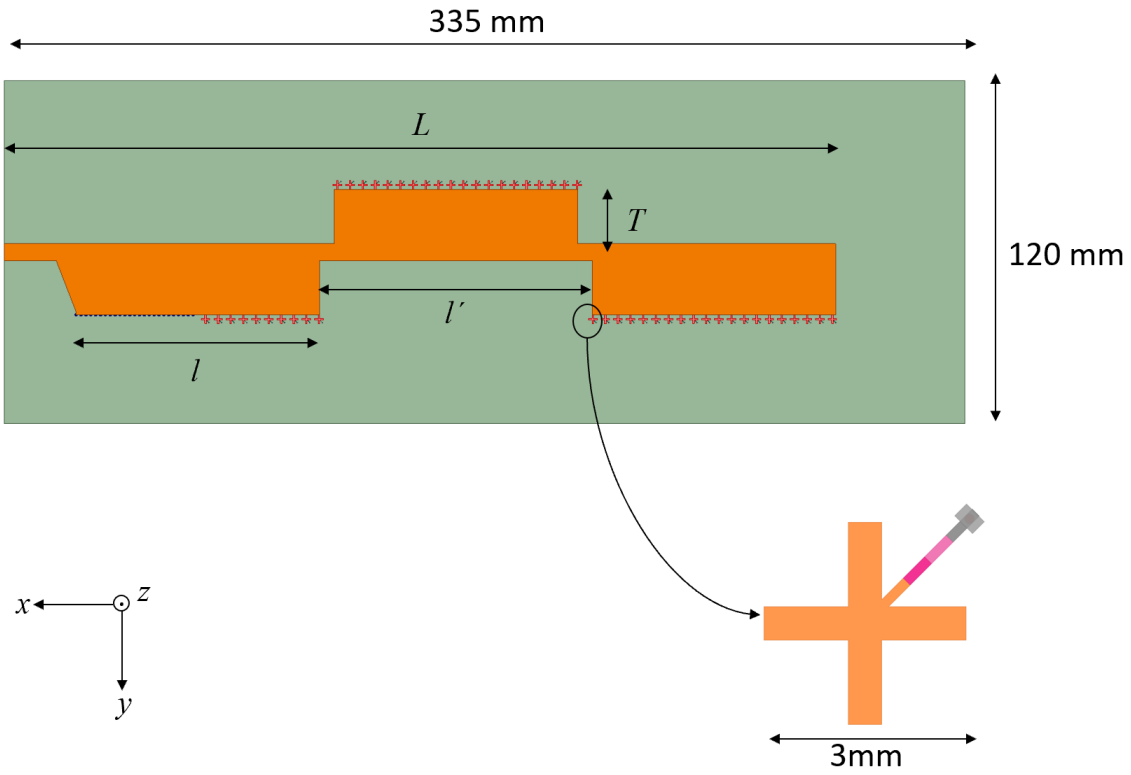

Fig. 4. 18: Final optimized antenna design with FPMS Unit cells (L = 290 mm, l = 85 mm, l' = 95 mm, T = 22 mm)

The continuous beam steering configuration of the final optimized antenna design is shown in the Fig. 4.19, with steering in right-hand side (backward) and left-hand side (forward) direction. The maximum gain attained is at 0° with a value of 10.5 dBi and a maximum variation of 2.5 dB. This kind of gain variation is expected from an antenna whose main-beam is steered from the direction of maximum radiation due to increase in the side lobe levels. Thus, the overall antenna results are quite promising and validate the concept of a reconfigurable antenna using FPMS technology.

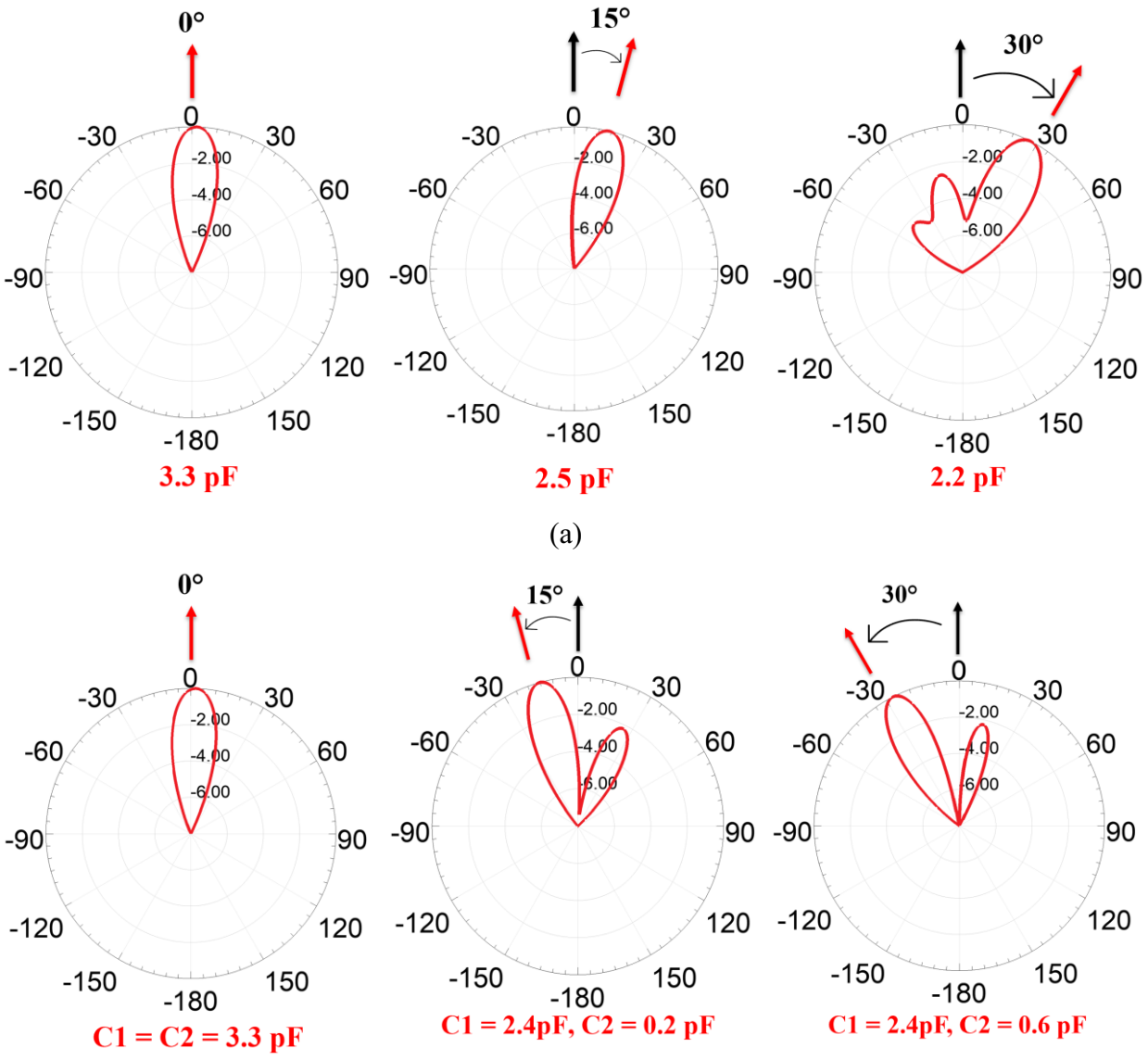

Fig. 4. 19: (a) Normalized radiation patter for right side beam steering (b) Normalized radiation pattern for left side beam steering

The antenna gain can further be increased with increase in the total length of the antenna. The simulated normalized radiation pattern of antenna with increased length (700mm) and a total of 7 patches, while keeping the width and thickness to be constant at 120mm and 3.962mm respectively is shown in Fig. 4.20. The radiation pattern shows a beam steering of ±30° with a maximum gain

of 13 dBi. Even though the antenna's gain has increased, the antenna's size is too large to be fabricated and realized.

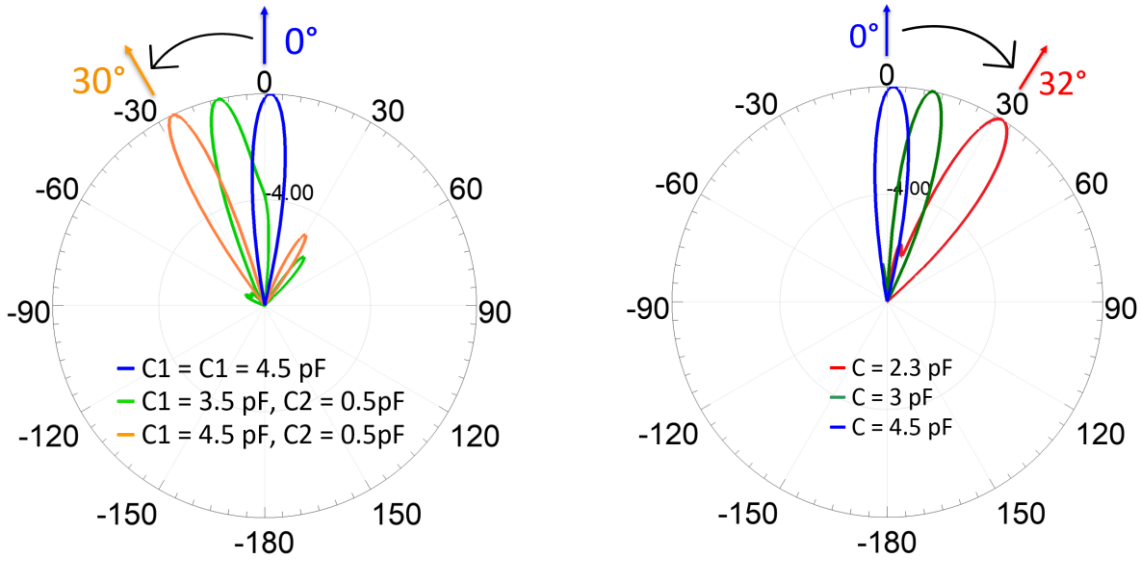

(a) (b)

Fig. 4. 20: Antenna with 7 patches (a) Normalized simulated beam steering on forward direction (b) Normalized simulation beam steering on backward direction

4.6 Comparison between the Analytical Model of MLWA and Simulated Results

The analytical/theoretical model explained in [38] for a periodic MLWA structure can be applied to validate the simulated results presented in this work. For this purpose, the dimensions of the antenna shown in Fig. 4.18 are used to evaluate Eq. (4.2) to (4.8). Since these equations can only be applied to a uniform permittivity substrate, Ansys HFSS is used to extract the effective permittivity ($\varepsilon_{eff.}$) experienced by the waves when propagating through the MLWA structure for

different values of capacitances on FPMS unit cells. These dielectric constant or permittivity values along with other antenna dimensions are then employed to determine the values of 'k_x' and the direction of maximum radiation of the antenna *'θ'* from the theory presented in section 4.2. As per the proposed theoretical model, for capacitance values of 2.2 pF, 2.5 pF and 3.3 pF, the extracted values of k_x and θ are plotted in Fig. 4.21. It is important to mention it here that these results are only obtained for the case when all the FPMS unit cells have same capacitance integrated on them. In the case where different capacitance values i.e., $C1$ and $C2$ are used on the two sides of the antenna, this theoretical model cannot be applied. The reason is because the effective permittivity for this case will be changing from one patch to the other. Therefore, a homogenous permittivity value cannot be used in the analytical model. Nonetheless, once the results for same capacitance values (2.2 pF, 2.5 pF, 3.3 pF) throughout the MLWA structure are obtained, it is necessary to compare them with the simulated results of Ansys HFSS model. To do so, Fig. 4.22 is shown here. A comparison between the theoretical values of θ and the simulated values is shown here. An excellent agreement can be observed between the theory and simulations, validating the proof of concept of an MLWA design based on FPMS technology.

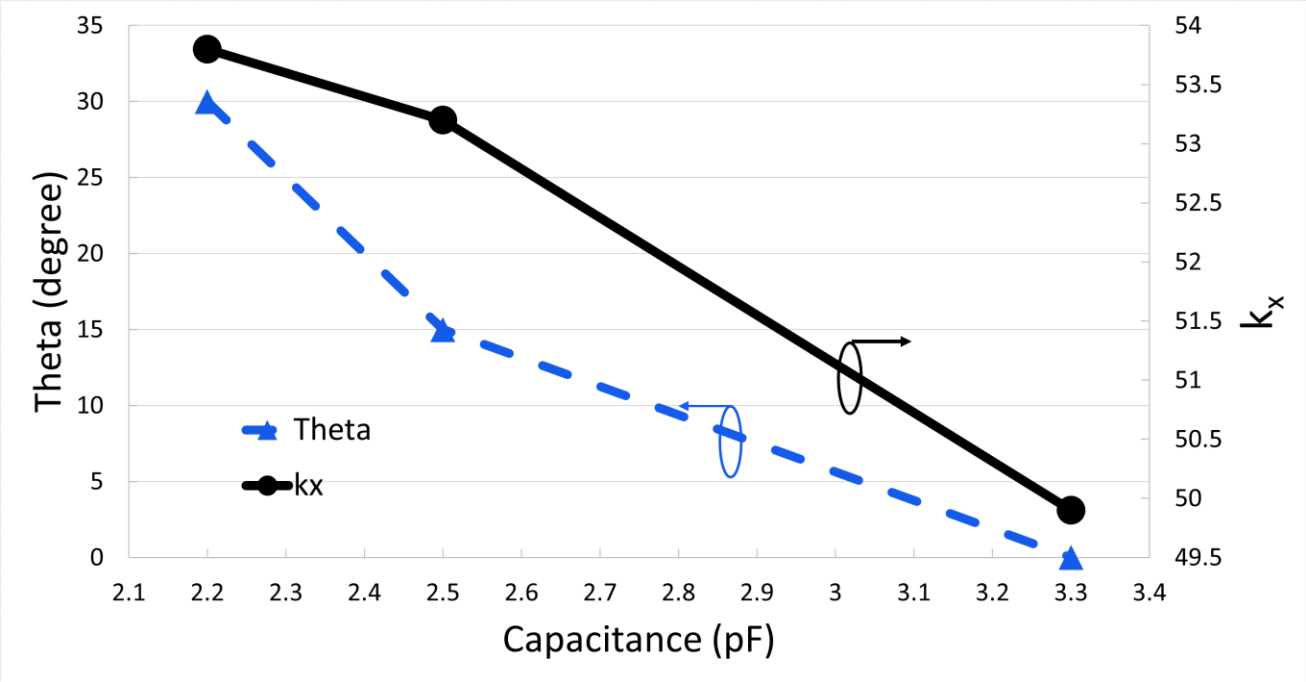

Fig. 4. 21: Theoretical results of antenna direction of radiation for different capacitance values of FPMS unit cell

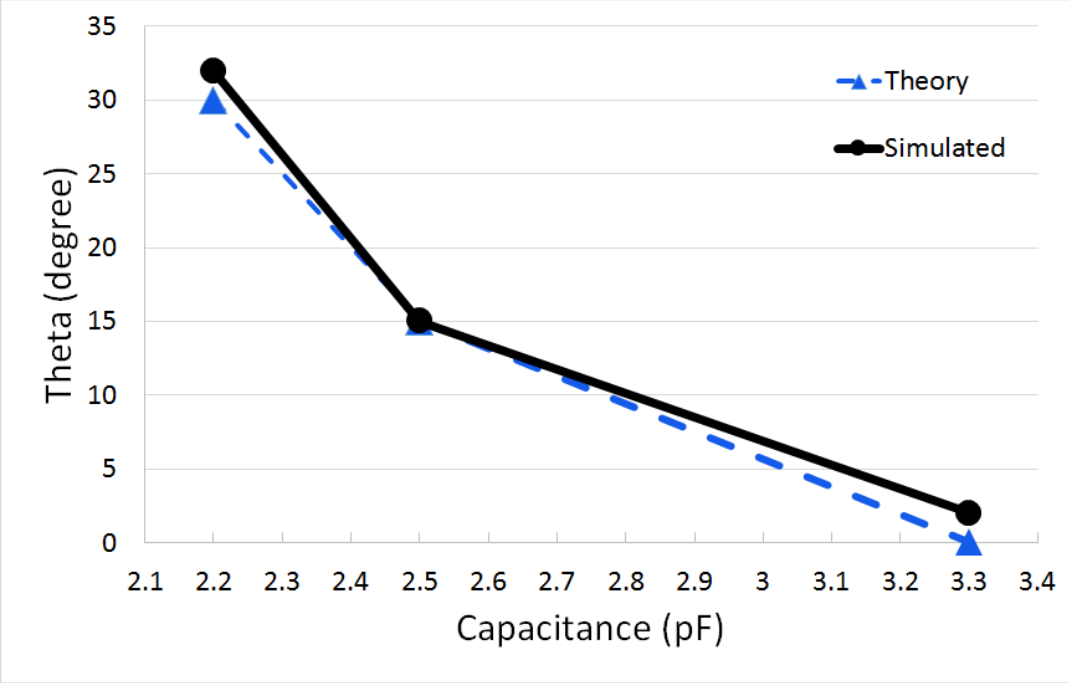

Fig. 4. 22: Comparison between the theory and simulations of FPMS based MLWA

4.7 Conclusion

A novel micro-strip-line based LWA design was demonstrated with reconfigurability in the form of radiation pattern with the implementation of FPMS unit cells. The reference antenna design is explained with the help of simulated results as well as its theoretical understanding is illustrated through this work. The optimize antenna has a total length of 335 mm and a width of 120 mm, showing a beam steering of ±30° with a maximum gain of 10.5 dBi and a minimum gain variation of 2.5 dB. The antenna has acceptable impedance matching for all its radiation values with a minimum reflection coefficient value of -11 dB. The gain of the antenna can further be doubled with the increase in length but will be hard to fabricate and realize.

Chapter 5

Conclusion and Future Work

5.1 Conclusions

The future of modern applications is uncertain without the inclusion of antenna design that is field reconfigurable, compact, and, last but not the least, efficient. This thesis presents one such modern antenna design with all of the aforementioned capabilities in the form of radiation pattern reconfigurability. A novel antenna design based on a microstrip line-based leaky wave antenna (MLWA) with integrated FPMS unit cell integration is reported in this thesis. For the first time, FPMS unit cells have been explored for their application in antenna designs. Therefore, this work can be considered as the stepping-stone towards a new class of antenna designs that can be regarded as 'Field Programmable Microwave Antennas (FPMA)'.

The antenna has a total length and width of 335 mm and 120 mm, respectively and is designed on a Duroid 5880 substrate. With effective integration of FPMS unit cells and by virtue of variable varactor values the antenna is allowed to steer its beam effectively at 2 GHz. A maximum gain of 10.5 dBi is achieved from the antenna with a gain variation of 2.5 dB.

The main lobe of the radiation can steer continuously from backward to forward direction by changing the capacitance values of the FPMS unit cells. A total beam steering of ±30° is obtained from Ansys HFSS full-wave simulations. Throughout the steering of antenna radiation, the antenna impedance remains matched which is highly desired for any antenna system. At the end, the theoretical model of an MLWA structure is used to validate these simulation results. The analytical model used here is presented in [38] and has already been proven using actual prototyping. This

gives a high degree of confidence that the proposed antenna design will provide the beam steering results as predicted by the simulation model.

5.2 Future Work

The first step to move forward in presenting a proof-of-concept of an FPMA design is the actual realization of the proposed FPMS based MLWA design. For this purpose, two vendors have been contacted to fabricate the antenna design. These vendors are Syber Circuits and Candor Inc. located near Toronto, ON. The quotation obtained from the first vendor is more feasible in terms of timeline and cost. The plan is to fabricate the antenna design using the facility of Syber Circuits after which the characterization will be carried out. For antenna measurements/characterization, it is desired to use the facility of Georgian College in Barrie, ON. However, at present the antenna anechoic chamber present at this facility is not ready for far-field measurements. It can only be used for Electromagnetic Compatibility (EMC) testing in its present state. Having said that, with some modifications the chamber can be employed for the far-field measurements of any antenna. Therefore, it is anticipated that the antenna design can be tested here. Secondary options include, Polytechnique Montreal (University of Montreal) and University of Waterloo both of which have operational anechoic chambers.

Once this design has been validated using actual antenna radiation pattern measurements, it is anticipated that more of other class of antennas are to be studied using FPMS technology. These include horn, lens and reflector antennas. On characteristic common among all the three antenna designs proposed here is that they rely on substrate properties to control the propagation of the wave through them. Also, their implementation is such that one can easily use the FPMS unit cells onto the body of the antenna to achieve the desired results. This can be easily explained by considering the example of a reflector antenna. A reflector antenna/surface is composed of many

antenna elements which are usually made up of same structure. The direction of main beam in such a design can be controlled by smartly maneuvering the relative phase shift between the antenna elements. If these elements are implemented using FPMS unit cells, then one can control the phase difference between consecutive elements by modulating the varactor diodes on each unit cell. As a result, a dynamic range of relative phase shift can be achieved that will allow the designer to conveniently steer the antenna beam. This concept is diagrammatically represented in Fig. 5.1.

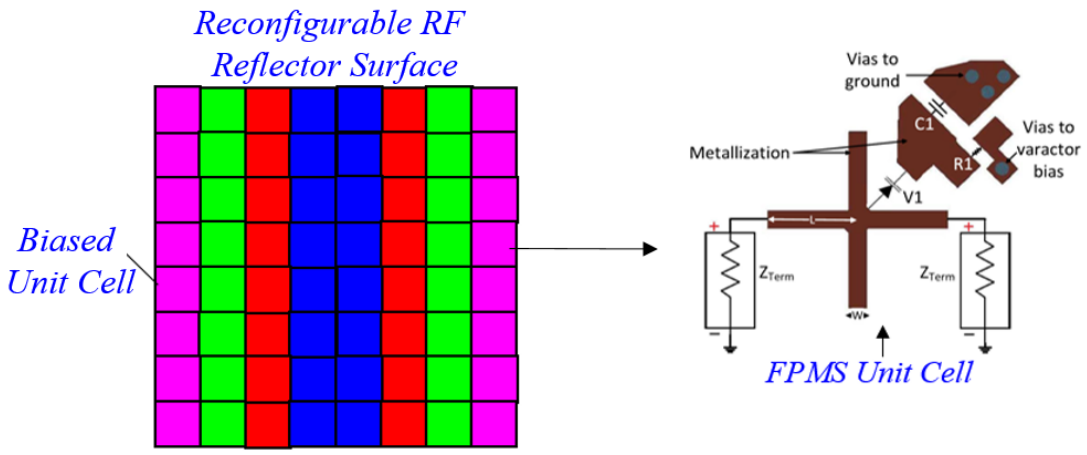

Fig. 5. 1: Reconfigurable RF reflector design and the physical model of the FPMS unit cell

The same concept can be applied to other antenna elements to provide reconfigurability in terms of antenna radiation, polarization, or impedance. Thus, this work opens the door for a completely new class of antenna that can be developed using FPMS technology.

Bibliography

[1] Zhi Ning Chen, Duixian Liu, Hisamatsu Nakano, Xianming Qing, Thomas Zwick, "HANDBOOK OF ANTENNA TECHNOLOGIES," *Springer Singapore*, 2016.

[2] http://www.microwaves101.com/encyclopedia/phasedarrays.cfm.

[3] Debabrata K. Karmokar, Karu P. Esselle and Trevor S. Bird, "Wideband Microstrip Leaky-Wave Antennas with Two Symmetrical Side Beams for Simultaneous Dual-Beam Scanning," *IEEE TRANSACTIONS ON ANTENNAS AND PROPAGATION,* Vol. 64, No. 4, April 2016.

[4] Debabrata K. et al., "Fixed-Frequency Beam Steering of Microstrip Leaky-Wave Antennas Using Binary Switches," *IEEE TRANSACTIONS ON ANTENNAS AND PROPAGATION,* June 2016.

[5] Efficient power conversion corporation "https://epc-co.com/epc/GaNTalk/Post/13749/GaN-Technology-for-the-Connected-Car".

[6] Chapter 7, "MODERN ANTENNA HANDBOOK by Constantine A. Balanis A".

[7] Ajay Kumar Tiwari, Seema Awasthi and Rajat Kumar Singh, "A Symmetrical Periodic Leaky-Wave Antenna With Backward-to-Forward Scanning," *IEEE ANTENNAS AND WIRELESS PROPAGATION LETTERS,* Vol. 19, No. 4, April 2020.

[8] Matthias Steeg, Asmaa Al Assad and Andreas Stöhr, "All Photonic Radar System based on Laser Frequency Sweeping and Leaky-Wave Antennas," 2018 International Topical Meeting on Microwave Photonics (MWP), December 2018.

[9] Premysl Hudec, Petr Panek, and Vojtech Jenik, "Multimode Adaptable Microwave Radar Sensor Based on Leaky-Wave Antennas," *IEEE TRANSACTIONS ON MICROWAVE THEORY AND TECHNIQUES*, Vol. 65, No. 9, September 2017.

[10] J. de Villiers and E. Barnard, "Backpropagation Neural Nets With One And Two Hidden Layers," *IEEE TRANS. NEURAL NETWORKS*, Vol. 4, pp. 136–141, January 1992.

[11] R. A. Sigelmann, and A. Ishimaru, "Radiation from Periodic Structures Excited by an Aperiodic Source," *IEEE TRANSACTIONS ON ANTENNAS AND PROPAGATION,* Volume: 13, Issue: 3, May 1965.

[12] W. ROTMANT AND A. A. OLINER, "Asymmetrical Trough Waveguide Antennas," *IRE TRANSACTIONS ON ANTENNAS AND PROPAGATION*, Volume: 7, Issue: 2, April 1959

[13] L. Goldstone and A. Oliner, "Leaky-Wave Antennas I: Rectangular Waveguides," *IRE TRANSACTIONS ON ANTENNAS AND PROPAGATION* (Volume: 7, Issue: 4, October 1959)

[14] R. C. HONEY "A Flush-Mounted Leaky-Wave Antenna With Predictable Patterns," *IRE TRANSACTIONS ON ANTENNAS AND PROPAGATION* (Volume: 7, Issue: 4, October 1959)

[15] S. Nishida, "Coupled leaky waveguides II: Two Parallel Slits In A Cylinder," *IRE TRANSACTIONS ON ANTENNAS AND PROPAGATION* (Volume: 8, Issue: 4, July 1960).

[16] L. O. Goldstone and A. A. Oliner, "Leaky Wave Antennas II: Circular Waveguides," *IRE TRANSACTIONS ON ANTENNAS AND PROPAGATION* (Volume: 9, Issue: 3, May 1961)

[17] A. A. Oliner, Scannable millimeter wave arrays, Final Report on RADC Contract No. F19628–84-K-0025, Polytechnic University, 30 September 1988.

[18] D. R. Jackson and A. A. Oliner, "A Leaky-Wave Analysis Of The High-Gain Printed Antenna Configuration," *IEEE TRANSACTIONS ON ANTENNAS AND PROPAGATION*, Vol. 36, pp. 905–910, July 1988.

[19] D. R. Jackson, A. A. Oliner, and A. Ip, "Leaky-Wave Propagation And Radiation For A Narrow-Beam Multiple-Layer Dielectric Structure," *IEEE TRANSACTIONS ON ANTENNAS AND PROPAGATION,* Vol. 41, pp. 344–348, March 1993.

[20] L. O. Goldstone and A. A. Oliner, "Leaky-wave antennas—Part I: Rectangular waveguides," *IRE TRANSACTIONS ON ANTENNAS AND PROPAGATION,* Vol. 7, pp. 307–319, October 1959.

[21] J. N. Hines and J. R. Upson, "A Wide Aperture Tapered-Depth Scanning Antenna," *OHIO STATE UNIVERSITY RESEARCH FOUNDATION*, Report 667–7, Columbus, OH, December 1957.

[22] A. Hessel, "General Characteristics Of Traveling-Wave Antennas," in Antenna Theory, Part 2 , R. E. Collin and F. J. Zucker (Eds.), McGraw-Hill, New York, 1969, Chap. 19.

[23] T. Tamir, Leaky-wave antennas, in Antenna Theory, Part 2, R. E. Collin and F. J. Zucker (Eds.), McGraw-Hill, New York, 1969, Chap. 20.

[24] Swati Majumder and David R. Jackson, "Radiation Characteristics Of One-Dimensional Periodic Leaky-Wave Antennas," *IEEE ANTENNAS AND PROPAGATION SOCIETY INTERNATIONAL SYMPOSIUM,* July 1997.

[25] Thomas Geibig, Alex Shoykhetbrod, Alexander Hommes, Reinhold Herschel, Nils Pohl, "Compact 3D Imaging Radar Based On FMCW Driven Frequency-Scanning Antennas," 2016 *IEEE Radar Conference* (RadarConf), June 2016

[26] Anirban Sarkar, Duc Anh Pham, and Sungjoon Lim, "Tunable Higher Order Mode-Based Dual-Beam CRLH Microstrip Leaky-Wave Antenna for V-Band Backward–Broadside–Forward Radiation Coverage," *IEEE TRANSACTIONS ON ANTENNAS AND PROPAGATION*, Vol. 68, No. 10, October 2020.

[27] Shyh-Jong Chung, Ming-yi Li, S. Kanamaluru, and Kai Chang, "Meander-Image-Line-Feed Microstrip Antenna Array For Frequency-Swept Beam Steering," *IEEE ANTENNAS AND PROPAGATION SOCIETY INTERNATIONAL SYMPOSIUM. 1996 DIGEST*, August 2002.

[28] Shujaat Ali Khan Tanoli, Mohammad Ismail Khan, Qaiser Fraz, Xiaodong Yang , and Syed Aziz Shah, "A Compact Beam-Scanning Leaky-Wave Antenna With Improved Performance," *IEEE ANTENNAS AND WIRELESS PROPAGATION LETTERS*, Vol. 17, No. 5, May 2018.

[29] Muhammad Zaka Ali and Qasim Umar Khan, "High Gain Backward Scanning Substrate Integrated Waveguide Leaky Wave Antenna," *IEEE TRANSACTIONS ON ANTENNAS AND PROPAGATION*, Vol. 69, No. 1, January 2021.

[30] Yuanxin Li, Quan Xue, Hong-Zhou Tan, and Yunliang Long, “The Half-Width Microstrip Leaky Wave Antenna With the Periodic Short Circuits,” *IEEE TRANSACTIONS ON ANTENNAS AND PROPAGATION,* Vol. 59, No. 9, September 2011.

[31] Yuanxin Li, Quan Xue, Edward Kai-Ning Yung, and Yunliang Long, “Fixed-Frequency Dual-Beam Scanning Microstrip Leaky Wave Antenna,” *IEEE ANTENNAS AND WIRELESS PROPAGATION LETTERS*, Vol. 6, 2007.

[32] Manisha Kahar, Ravi Shaw, and Mrinal Kanti Mandal, “Fixed Frequency Electronically Beam Steering Microstrip Comb Line Antenna,” *2017 PROGRESS IN ELECTROMAGNETICS RESEARCH SYMPOSIUM,* Nov. 2017.

[33] S. Keyrouz, G. Perotto and H. J. Visser, “Lumped-Elements Tunable Frequency Selective Surfaces,” *THE 8TH EUROPEAN CONFERENCE ON ANTENNAS AND PROPAGATION*. September 2014.

[34] Tayfun Nesimoglu and Cumali Sabah, “A Tunable Metamaterial Resonator Using Varactor Diodes to Facilitate the Design of Reconfigurable Microwave Circuits,” *IEEE TRANSACTIONS ON CIRCUITS AND SYSTEMS—II: EXPRESS BRIEFS,* Vol. 63, No. 1, January 2016.

[35] Marina Villalba Carballo, Dubari Borah and T.S.Kalkur, “U-Slot Dual-band Frequency Reconfigurable Patch Antenna Tuned With Commercial Ferroelectric BST capacitors,” 2019 *IEEE INTERNATIONAL CONFERENCE ON MICROWAVES, ANTENNAS, COMMUNICATIONS AND ELECTRONIC SYSTEMS (COMCAS).* January 2020.

[36] Nathan Jess, Barry A. Syrett, and Langis Roy, "The Field-Programmable Microwave Substrate," *IEEE TRANSACTIONS ON MICROWAVE THEORY AND TECHNIQUES*, Vol. 64, No. 11, November 2016.

[37] Alexandre Natã, Vicente Gustavo Maciulis Dip and Cynthia Junqueira, “The Step-By-Step Development Of NRW Method,” *2011 SBMO/IEEE MTT-S INTERNATIONAL MICROWAVE AND OPTOELECTRONICS CONFERENCE* (IMOC 2011).

[38] Yuanxin Li, Quan Xue, Edward Kai-Ning Yung, and Yunliang Long, "The Periodic Half-Width Microstrip Leaky-Wave Antenna With a Backward to Forward Scanning Capability," *IEEE TRANSACTIONS ON ANTENNAS AND PROPAGATION*, Vol. 58, No. 3, March 2010.

[39] C. Luxey and J. M. Laheurte, "Simple Design Of Dual-Beam Leaky-Wave Antennas In Microstrips", *Proc. Inst. Elect. Eng. Microw. Antennas Propag.*, vol. 144, no. 6, pp. 397-402, Dec. 1997.

[40] A. K. Bhattacharyya, "Long Rectangular Patch Antenna With A Single Feed", *IEEE TRANSACTIONS ON ANTENNAS AND PROPAGATION*, vol. 38, no. 7, pp. 987-993, Jul. 1990.